UCRL-10770

University of California

Ernest O. Lawrence Radiation Laboratory

TWO-WEEK LOAN COPY

This is a Library Circulating Copy which may be borrowed for two weeks. For a personal retention copy, call Tech. Info. Division, Ext. 5545

INVERSION MATRIX FOR A HELIUM-3 FAST-NEUTRON SPECTROMETER

Berkeley, California

DISCLAIMER

This document was prepared as an account of work sponsored by the United States Government. While this document is believed to contain correct information, neither the United States Government nor any agency thereof, nor the Regents of the University of California, nor any of their employees, makes any warranty, express or implied, or assumes any legal responsibility for the accuracy, completeness, or usefulness of any information, apparatus, product, or process disclosed, or represents that its use would not infringe privately owned rights. Reference herein to any specific commercial product, process, or service by its trade name, trademark, manufacturer, or otherwise, does not necessarily constitute or imply its endorsement, recommendation, or favoring by the United States Government or any agency thereof, or the Regents of the University of California. The views and opinions of authors expressed herein do not necessarily state or reflect those of the United States Government or any agency thereof or the Regents of the University of California.

Research and Development

UCRL-10770
UC-34 Physics
TID-4500 (19th Ed.)

UNIVERSITY OF CALIFORNIA
Lawrence Radiation Laboratory
Berkeley, California

Contract No. W-7405-eng-48

INVERSION MATRIX FOR A HELIUM-3 FAST-NEUTRON SPECTROMETER

Hsien-Tsan Wang
(M.S. Thesis)

April 23, 1963

Printed in USA. Price $2.25. Available from the
Office of Technical Services
U. S. Department of Commerce
Washington 25, D.C.

INVERSION MATRIX FOR A HELIUM-3 FAST-NEUTRON SPECTROMETER

Contents

Abstract v

I. Introduction 1

II. Wall-Effect

A. Analysis 4

B. The Probability, $P(E \rightarrow E_i)$, per Unit Energy that Reaction Products of Energy E Will Deposit Energy E_i Inside the Sensitive Volume Due to Wall Effects . 13

III. Wall Effect of Protons and Tritons

A. Energy of Protons and Tritons 15

B. The Probability that Protons or Tritons Will Not Hit the Counter Wall 27

C. Consideration of Two Simultaneously Emitted Protons and Tritons 35

D. Unfolding of the Wall Effect of Protons and Tritons . . 36

IV. Recoil Effect

A. Recoil Cross Sections 39

B. Energy of Recoiled Nuclei 44

C. The Probability, $P(E_r)$, per Unit Energy that a Neutron of Energy E Undergoing the Reaction $He^3(n, n)He^3$ Will Cause that Helium-3 Nucleus to Recoil with Energy E_r 46

D. Unfolding of Recoil Effects 47

V. Effect of the Reaction $He^3(n, d)D$

A. Reaction Energy 52

B. Unfolding of the $He^3(n, d)D$ Effects 54

VI. Inversion Matrix

A. Spectrometer Efficiency 62

B. Recombination Considerations 68

C. The Matrix 68

D. The Corrected Spectrum 70

VII. Sample Calculation
A. The Detector 77
B. The Raw Spectrum 77
C. Unfolding Procedures 79
D. Comparison of Results 91
Acknowledgments 94
Appendices
A. Computer Program 95
B. Sample Calculation 102
References 105

INVERSION MATRIX FOR A HELIUM-3 FAST-NEUTRON SPECTROMETER

Hsien-Tsan Wang

Lawrence Radiation Laboratory
University of California
Berkeley, California

April 23, 1963

ABSTRACT

A general method for calculating the inversion matrix for a helium-3 fast-neutron spectrometer is obtained here by analyzing the wall effect, the recoil effect, and the $He^3(n, d)D$ effect. The dependence of the inversion matrix and the counter efficiency on the filling-gas pressure and the counter dimensions is also presented. A computer program that computes the response matrix and inverts it for the case of a 10- atmosphere-pressure neutron detector is included as an example.

I. INTRODUCTION

Because of its ability to discriminate against γ rays, the He^3 fast-neutron counter using the $He^3(n,p)T$ reaction has drawn the interest of investigators from many fields. A number of papers regarding the use of He^3 counters for investigation and experimentation have been published,[1-6] and now the He^3 detector is commercially available. However, the use of most He^3 counters has been limited to neutron energies below 1 MeV by two factors: first, the ambiguity that arises when neutrons with more than 1 MeV make He^3 recoils whose pulse heights are the same as those of the protons produced by lower-energy neutrons in the $He^3(n,p)T$ reaction, and second, the difficulty in removing wall effects.

In a rather successful attempt to raise the useful energy range of a He^3 counter, a special design known as a wall-less counter has recently been developed by Brown.[5] He uses a peripheral ring of 16 small counters to eliminate the cylindrical wall effects and to unfold the He recoil from the competing processes. The useful range of the counter with this method is as high as 10 MeV.

This paper primarily treats the wall effect in an ordinary He^3 gas-filled detector. Based on this analysis, a method of computing the original spectrum from the known response spectrum by using an inversion matrix is presented here for inverting the raw spectrum recorded by the ordinary He^3 gas-filled detector to a "resultant"* proton pulse-height (without wall effect) spectrum due to the $He^3(n,p)T$ reaction. The "corrected" neutron spectrum is then obtained from this inverted spectrum divided by the counter efficiency.

---

* The "resultant" proton pulse-height spectrum is defined as the spectrum produced by tracks of protons which do not hit the counter wall; this special nomenclature will be used later and refers to the same thing.

The recorded pulse-height spectrum is due to the deposition of energy from all possible charged particles from all the possible reactions of neutrons with He^3. These possible reactions, which are energy-dependent, are as follows:

a. $He^3(n, p)T$ for neutrons of all energies.

b. $He^3(n, n)He^3$ for neutrons of all energies.

c. $He^3(n, d)D$ for neutrons of energy $\geqslant 4.36$ MeV.

d. $He^3(n, p, n)D$ for neutrons of energy $\geqslant 7.32$ MeV.

e. $He^3(n, p, 2n)H^1$ for neutrons of energy $\geqslant 10.3$ MeV.

All of the tracks of these charged particles can of course be cut short by the counter walls producing the wall effects that we must unfold from the desired spectrum. Therefore the recorded raw spectrum is actually a complicated combination of all of these pulse heights.

In order to unfold all of the extraneous pulse-height spectra from the resultant (without the wall effect) proton spectrum due to (n, p) events, the following scheme is used:

a. General analysis of wall effect.

b. Analysis of the wall effect due to protons.

c. Analysis of helium nucleus recoils and their wall effect.

d. The analysis of deuterons and their wall effect.

After unfolding all of the above effects the final result will be the desired resultant (n, p) spectrum, which can be approximately calculated by a machine computation method. In most detectors, a mixture of He^3 gas and krypton gas is used to provide increased stopping power for the protons. This has been taken into account by computing the range of charged particles in the gas mixture.

The dependence of filling-gas pressure and counter size have also been considered. Due to the unavailability of cross sections for such reactions as $He^3(n, p, n)D$ and $He^3(n, p, 2n)H^1$ their effects are not calculated here. However, following a procedure similar to that used here, the calculation will be straightforward whenever these cross sections become available.

In order to show the application of this method, a computation is included to illustrate the unfolding of the spectrum of a 10-atmosphere He^3-filled commercial detector.

Finally, it should be mentioned here that the study reported herein is essentially an extension of the work of Brown,[5] i.e., the wall effects on the spectrum are corrected in addition to the corrections developed in Brown's work. For the purpose of utilizing his results to the maximum extent, the analysis presented here follows his method very closely. A number of his graphs, drawings, and equations concerning the reaction cross sections, the energies of particles in question, and the probability of particle tracks not hitting the counter walls are also included here for completeness and for direct reference in later applications. These materials, some of which are added with a more detailed description or derivation, are all indicated herein by a "dagger" (†).

As a result of close application of his derivation—as well as taking the wall effects into account—it is found (a) that one newly developed term has to be added to each formula in each case (i.e., his formulas of deuteron effects or recoil effects) and (b) that one additional formula has to be developed here to take into account the wall effect due to protons and tritons. This effect was completely eliminated in Brown's work by using an anticoincident counting technique. The important step of taking wall effects into account is based on the development of a new probability function $P(E \rightarrow E_i)$; this is the probability per unit energy that the reaction products of energy E will deposit energy E_i inside the sensitive volume due to the wall effect (see discussion in Subsec. II. B.)

II. WALL EFFECT

The wall effect in the detector arises when ionizing tracks pass out of the sensitive volume through the wall. This action results in a loss of events at the original spectral energy and the coincident appearance of extraneous events at lower energies.

A. Analysis

The analysis is based on the following assumptions:

a. The nuclear-reaction site density is uniformly distributed throughout the volume of the detector.

b. The charged particles are expelled from the nuclear reaction in an isotropic laboratory (lab) distribution.

c. For the first-order approximation the charged particles produce tracks along which the specific ionization is constant; i. e., the pulse height produced is proportional to the length of the track falling inside the sensitive volume of the detector. This assumption can be fairly well justified from the curves of Figs. 39 and 40, the range-energy curve for protons in helium. Based on these curves, the assumption introduces no essential error in the the energy range from 3 to 30 MeV. In the energy range from 0 to 3 MeV, the error due to this assumption can be limited to within 5% if a proper proportional constant is chosen for this assumption.

The usual configuration of cylindrical gas-filled detectors will have a form as in Fig. 1. The sensitive volume of this detector is measured by the counting-wire length L, while the actual gas-filled

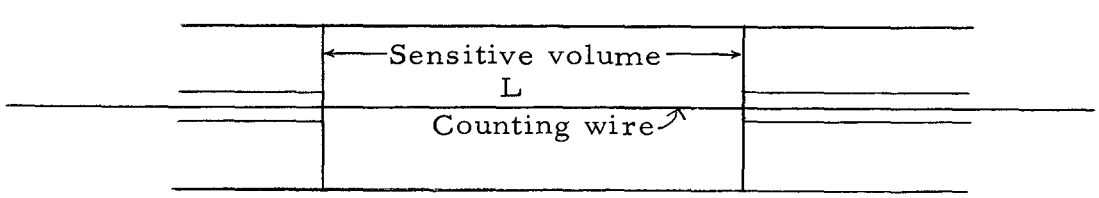

Fig. 1.

volume will also include the volume of the counting-wire insulation, which provides insulation between the counting wire and detector wall and gives more uniform electric field along the wire.

The geometry of analysis is given in Fig. 2.

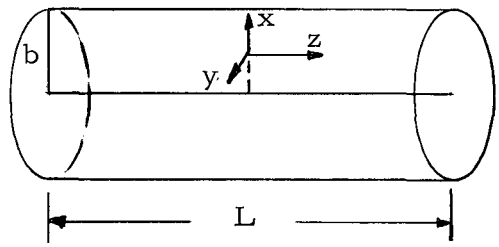

Fig. 2.

Choose the reaction site as the origin of the coordinate system. Then the origin is at a distance r from the counting wire, the z axis is parallel to the counter axis, the radius of the counter is b. Assume the track length of charged particles is ℓ. For the analysis the whole gas-filled volume of the detector can be divided into four regions, which will be defined in the subsequent discussion.

1. Region A

Region A is the core of the sensitive volume defined by radius of $b-\ell$ and length $L-2\ell$, as shown in Fig. 3 where ℓ is the track length of charged particles.

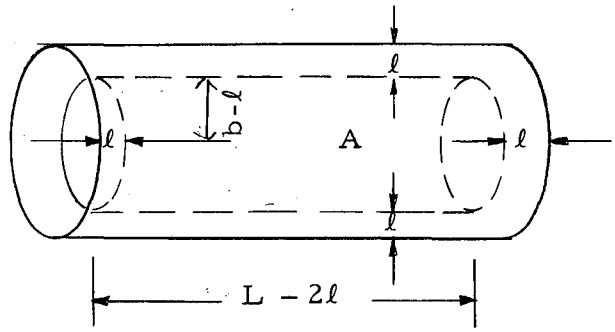

Fig. 3.

It is clear that only tracks of "full size"* can be formed in this region. Therefore, the probability $p_A(\rho)$ per unit track length, that a track will have a length between ρ and $\rho + d\rho$, in this region is

$$p_A(\rho)d\rho = \delta(\rho - \ell)d\rho.$$

Then for a single reaction happening in region A the probability is

$$\int_0^\infty p_A(\rho)d\rho = \int_0^\infty \delta(\rho - \ell)d\rho = 1.^\dagger$$

2. Region B

Region B is the hollow cylindrical volume with an inner radius of $b-\ell$, an outer radius of b, and a length of $L-2\ell$, as in Fig. 4.

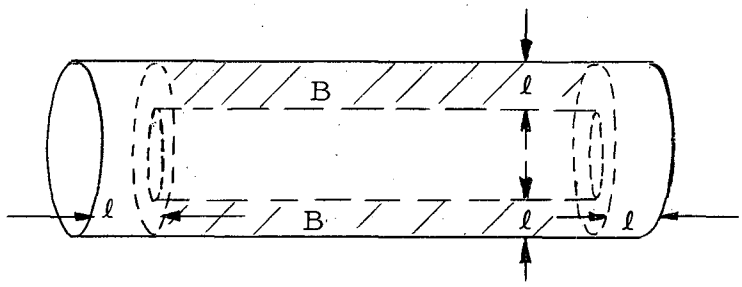

Fig. 4.

* The "full size" track of a charged particle is defined here as the track length of that charged particle which deposits all of its energy inside the sensitive volume of the detector; or in other words, it is the track of a charged particle falling completely inside the sensitive volume without hitting the walls of the counter. And the spectrum due to different "full size" tracks is called a resultant spectrum as defined before.

The track length can be classified into two different cases:

Case 1.

From a single reaction in this region, those tracks not intersecting the wall will have length ℓ, the full-size track. The probability, $p_{B1}(\rho)$, per unit track length that a track will have a length between ρ and $(\rho + d\rho)$ in this region is

$$p_{B1}(\rho)d\rho = F_{B1}(\rho)\delta(\rho-\ell) \qquad \text{(II. 1)}^{\dagger}$$

where the factor $F_{B1}(\rho)$ represents the fractional area of a sphere with radius ℓ centered at (0, 0, 0) that falls inside the sensitive volume.

Referring to Fig. 5, it is seen that the fractional surface area of the sphere inside the cylinder is

$$F_{B1}(\rho) = \frac{4\pi\ell^2 - \int_S \ell^2 \sin\alpha\, d\alpha\, d\beta}{4\pi\ell^2} = 1 - \frac{1}{2}\int_{\alpha_1}^{\alpha_2} \sin\alpha\, d\alpha$$

$$= 1 - \frac{1}{4}\left[\left(\frac{b^2-\ell^2}{2\ell}\right)\frac{1}{r} + \left(\frac{b}{\ell}-2\right) - \left(\frac{3}{2\ell}\right) r\right], \qquad \text{(II. 2)}^{*\dagger}$$

where S = spherical surface area outside of the cylinder. Therefore

$$p_{B1}(\rho)d\rho = \left\{1 - \frac{1}{4}\left[\left(\frac{b^2-\ell^2}{2\ell}\right)\frac{1}{r} + \left(\frac{b}{\ell}-2\right) - \frac{3r}{2\ell}\right]\right\}\delta(\rho-\ell)d\rho \qquad \text{(II.3)}^{\dagger}$$

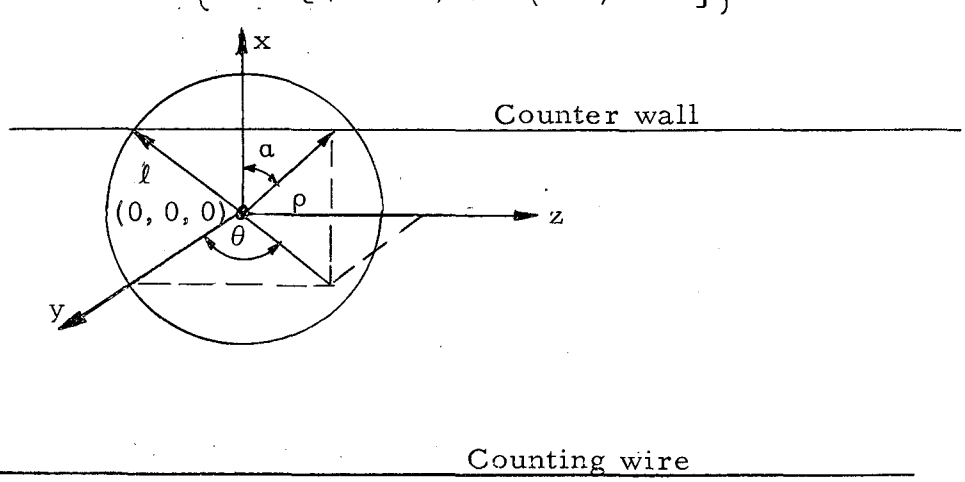

Fig. 5.

* For the detailed derivation of $F_{B1}(\rho)$ see Subsec. III. A.

Case 2.

Those tracks that do intersect the detector wall will lose a fraction of their length. The probability of hitting the wall is then the spherical surface outside of the cylinder:

$$p_{B2}(\rho)d\rho = \frac{\int_S \ell^2 \sin\alpha\, d\alpha\, d\beta}{4\pi\ell^2} = \frac{\int_0^{2\pi} d\beta \sin\alpha\, d\alpha}{4\pi} = \frac{1}{2}\sin\alpha\, d\alpha. \qquad \text{(II. 4)}^{\dagger}$$

Since

$$\rho = \frac{b-r}{\cos\alpha}, \quad \sin\alpha\, d\alpha = \frac{b-r}{\rho^2}\, d\rho \qquad \text{(II. 5)}$$

then

$$p_{B2}(\rho)d\rho = \frac{1}{2}\frac{b-r}{\rho^2}\, d\rho. \qquad \text{(II. 6)}^{\dagger}$$

3. Region C

Regions C are the portions of the sensitive volume of distance ℓ from the ends of the sensitive volume, as in Fig. 6.

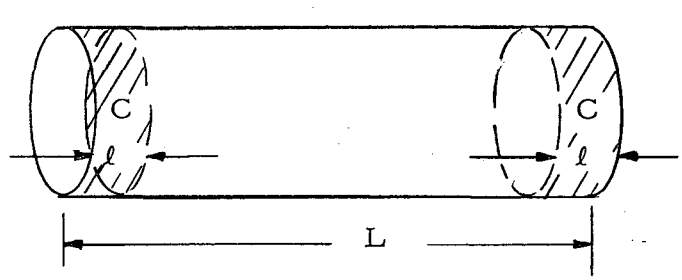

Fig. 6.

The track length can be classified into two different cases:

Case 1.

For a simple reaction in this region, the probability of having a full track length ℓ is

$$p_{C1}(\rho)d\rho = F_{C1}(\rho)\,\delta\,(\ell - \rho)\,d\rho\ , \qquad \text{(II.7)}$$

where

$$F_{C1}(\rho) = \frac{4\pi\ell^2 - \iint_{SC} \sin\alpha\, d\alpha\, d\beta}{4\pi\,\ell^2} = 1 - \frac{1}{2}\int_{\alpha} \sin\alpha\, d\alpha$$

$$= 1 - \frac{1}{2}\,[\cos\alpha]_{\cos^{-1} Z/\ell}^{0}$$

$$= 1 - \frac{1}{2}\,[1 - \frac{Z}{\ell}] = \frac{1}{2}\,(1 + \frac{Z}{\ell}) \qquad \text{(II.8)}^{\dagger}$$

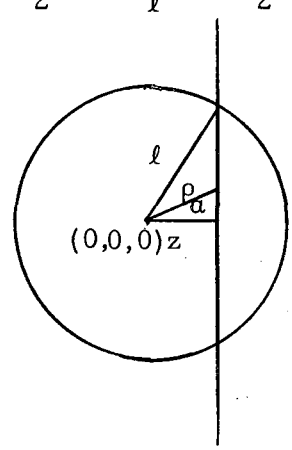

Case 2.

The probability of having a curtailed track length due to the wall effect is

$$p_{Cz}(\rho)\,d\rho = (\frac{1}{2}\sin\alpha\, d\alpha)\times 2.$$

Since $\cos\alpha = Z/\rho$, $\sin\alpha\, d\alpha = (Z/\rho^2)d\rho$; therefore

$$p_{C2}(\rho)d\rho = \frac{Z}{\rho^2}\,d\rho. \qquad \text{(II.9)}$$

4. Region D

Regions D are the portions of the gas-filled volume beyond the sensitive volume, as in Fig. 7.

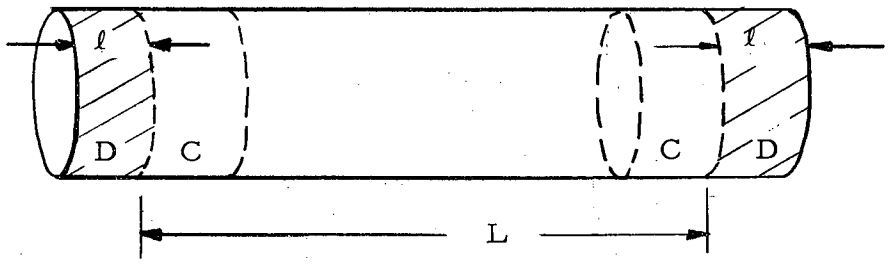

Fig. 7

Nuclear reactions occurring at sites outside the ends of sensitive volume can also cause energy to be deposited inside the sensitive volume of the counter.

If the probability of depositing energy from a track length inside the sensitive volume per unit track length of ρ is $p_D(\rho)$, then

$$p_D(\rho)d\rho = \left(\frac{1}{z} \sin\alpha\, d\alpha\right)\times 2,$$

but

$$\cos\alpha = -\frac{Z}{\rho - \ell},$$

therefore

$$\sin\alpha\, d\alpha = -\frac{Z}{(\ell - \rho)}\, d\rho \text{ for } \ell > \rho, \text{ and}$$

$$p_D(\rho)d\rho = \frac{Z d\rho}{(\ell - \rho)^2} \text{ for } (\ell - Z) \geqslant \rho \geqslant 0. \qquad \text{(II.10)}$$

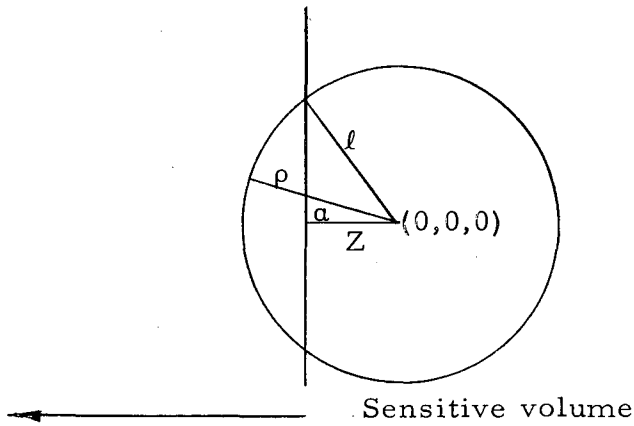

5. Summary of the General Wall Analysis

For an arbitrary track length ℓ the gas-filled volume can be divided into four regions, as in Fig. 8.

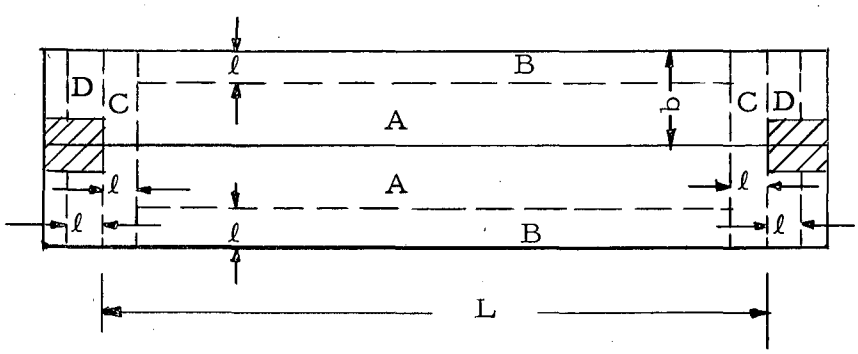

Fig. 8.

The probabilities per unit track length that a track will have a length between ρ and $(\rho + d\rho)$ in each region are listed in Table I.

Table I. Probability functions for different regions of the counter.

Region	Probability of giving full track length	Probability of giving partial track length due to wall effect
A	$p_A(\rho) = \delta(\rho-\ell)$	-
B	$p_{B1} = \left\{1 - \frac{1}{4}\left[\left(\frac{b^2-\ell^2}{2\ell}\right)\frac{1}{r} + \left(\frac{b}{\ell} - 2\right) - \frac{3r}{2\ell}\right]\right\}\delta(\rho-\ell)$	$p_{B2}(\rho) = \frac{1}{2}\,\frac{b-r}{\rho^2}$
C	$p_{C1} = (1 + \frac{Z}{\ell})\,\delta(\rho-\ell)$	$p_{C2}(\rho) = \frac{Z}{\rho^2}$
D	-	$p_{D2}(\rho) = \frac{Z}{(\ell-\rho)^2}$

B. The Probability, $P(E \rightarrow E_i)$, per Unit Energy that Reaction Products of Energy E Will Deposit Energy E_i Inside the Sensitive Volume Due to the Wall Effect

According to the foregoing analysis, now, if we assume that the pulse height is proportional to the energy deposited inside the sensitive volume, then it is reasonable to assume, for the first-order approximation, that

$$E = K,$$
$$E_i = K\rho,$$
$$E_b = Kb,$$
$$E_L = KL,$$

where K is some proportionality constant that will be cancelled out shortly. Therefore

$$P(E \rightarrow E_i) = K' p(\ell \rightarrow \rho),$$

where K' is another proportionality constant. For the whole counter

$$p(\ell \rightarrow \rho) = \int_{b-\ell}^{b} p_{B2}(\rho, r) g_1(r) dr + \int_0^{\ell} p_{C2}(\rho, z) g_2(z) + \int_0^{\ell} p_{D2}(\rho, z)\, g_3(z) dz. \qquad \text{(II.11)}$$

From Subsec. II. A,

$$p_{B2} = \frac{1}{2} \frac{b-r}{\rho^2}, \quad p_{C2} = \frac{z}{\rho^2}, \quad p_{D2} = \frac{z}{(\ell-\rho)^2},$$

and the volume fractions are, respectively,

$$g_1(r)dr = \frac{2\pi r dr}{\pi b^2} = \frac{2r dr}{b^2},$$

$$g_2(z)dz = g_3(z)dz = \frac{dz}{L},$$

therefore

$$p(\ell-\rho) = \int_{b-\ell}^{b} \frac{b-r}{\rho^2}\,\frac{r}{b^2}\,dr + \int_0^{\ell} \frac{z}{\rho^2}\,\frac{dz}{L} + \int_0^{\ell} \frac{z}{(\ell-\rho)^2}\,\frac{dz}{L}$$

$$= \left[\frac{1}{2b^2\rho^2}\left(b\ell^2 - \frac{2}{3}\ell^3\right) + \frac{\ell^2}{2\rho^2 L} + \frac{1}{2L}\right],$$

and since $\qquad p(\ell \to \rho)d\rho = P(E \to E_i)dE,$

then

$$P(E \to E_i) = \left[\frac{1}{2E_0^{\,2}E_i^{\,2}}\left(E_b E^2 - \frac{2}{3}E^3\right) + \frac{E^2}{2E_L E_i^{\,2}} + \frac{1}{2E_L}\right] \qquad \text{(II.12)}$$

This function will be used later.

III. WALL EFFECT OF PROTONS AND TRITONS

A. Energy of Protons and Tritons

The wall effect due to protons and tritons in the detector arises when protons or tritons pass out of the sensitive volume of the detector. Before going to the unfolding of the wall effect, let us first investigate the energy distribution of the protons and tritons. Protons and tritons in a He^3 neutron detector come from the reaction

$$ {}_2He^3 + {}_0n^1 = {}_1p^1 + {}_1T^3 + Q, \qquad \text{(III.1)} $$

where the reaction energy Q = 0.764 MeV is determined from the masses ot these particles in this reaction. If E_n is the neutron energy in the laboratory system (lab), then, the neutron energy in the center of mass (c. m.) system $(E_n)_{c.m.}$ is

$$ (E_n)_{c.m.} = \frac{m_{He^3}}{m_{He^3}+m_n} E_n = \frac{3}{4} E_n. \qquad \text{(III.2)} $$

The total energy delivered to reaction products in the c. m. system is

$$ \frac{3}{4} E_n + Q. \qquad \text{(III.3)} $$

This energy is divided between the protons and tritons in c. m. as follows:

$$ (E_p)_{c.m.} = \frac{3}{4} \left(\frac{3}{4} E_n + Q \right), \qquad \text{(III.4)} $$

$$ (E_T)_{c.m.} = \frac{1}{4} \left(\frac{3}{4} E_n + Q \right) \qquad \text{(III.5)} $$

In the lab system, the total energy deposited is

$$ E_n + Q. \qquad \text{(III.6)} $$

This energy is divided between these two reaction products in a manner dependent on their masses and the angle of emission (see Fig. 9):

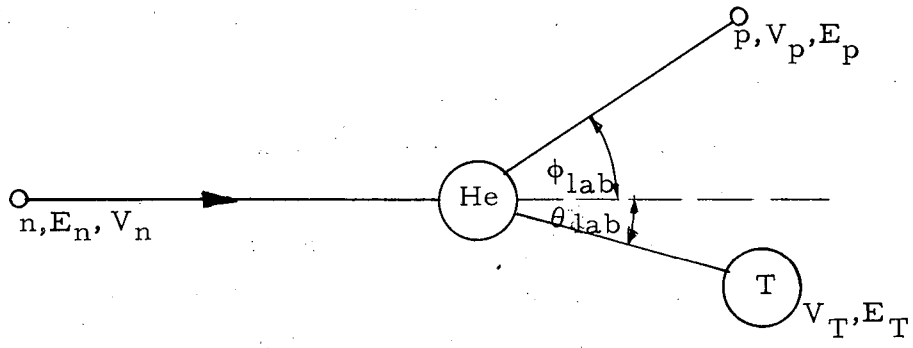

Fig. 9.

From the conservation of momentum

$$m_n V_n = m_p V_p \cos\phi_{lab} + m_T V_T \cos\theta_{lab}, \tag{III.7}$$

$$m_p V_p \sin\phi_{lab} = m_T V_T \sin\theta_{lab}. \tag{III.8}$$

From the conservation of energy

$$E_T + E_p = E_n + Q \tag{III.9}$$

and by using the relations $mV = (2mE)^{1/2}$, for each particle, we can easily derive

$$(E_p)_{lab} = \frac{E_n}{16}\left[\cos\phi_{lab} + \left(8 + \frac{12Q}{E_n} + \cos^2\phi_{lab}\right)^{1/2}\right]^2 \tag{III.10}$$

and

$$(E_T)_{lab} = \frac{3E_n}{16}\left[\cos\theta_{lab} + \left(\frac{4Q}{3E_n} + \cos^2\theta_{lab}\right)^{1/2}\right]^2. \tag{III.11}$$

The angular cross section in the lab system is obtained from

$$\left(\frac{d\sigma}{d\Omega}\right)_{lab} d\Omega_{lab} = \left(\frac{d\sigma}{d\Omega_{c.m.}}\right)_{c.m.} d\Omega_{c.m.}, \tag{III.12}$$

where $d\Omega = 2\pi d\mu$ (μ is the cosine of the angle in question).

If the particles are emitted isotropically in the c. m. system, then

$$\left(\frac{d\sigma}{d\Omega_{c.m.}}\right)_{c.m.} = \frac{1}{4\pi} , \qquad \text{(III.13)}$$

therefore

$$\left(\frac{d\sigma}{d\Omega}\right)_{lab} = \frac{1}{4\pi} \frac{d\Omega_{c.m.}}{d\Omega_{lab}} = \frac{1}{4\pi} \frac{d\mu_{c.m.}}{d\mu_{lab}} \qquad \text{(III.14)}$$

Since $\mu_{c.m.}$ and μ_{lab} are related (Fig. 10),

$$\mu_{c.m.} = \cos\theta_{c.m.} ,$$

$$\mu_{lab} = \cos\theta_{lab} ,$$

$$\mu_{lab} = \frac{V_{c.m.} + (V_p)_{c.m.}\,\mu_{c.m.}}{\left[(V_p{}^2)_{c.m.} + V^2_{c.m.} + 2(V_p)_{c.m.}\,V_{c.m.}\,\mu_{c.m.}\right]^{1/2}} ,$$

$$= \frac{\dfrac{V_{c.m.}}{(V_p)_{c.m.}} + \mu_{c.m.}}{\left\{1 + \left[\dfrac{V_{c.m.}}{(V_p)_{c.m.}}\right]^2 + 2\left[\dfrac{V_{c.m.}}{(V_p)_{c.m.}}\right]\mu_{c.m.}\right\}^{1/2}} .$$

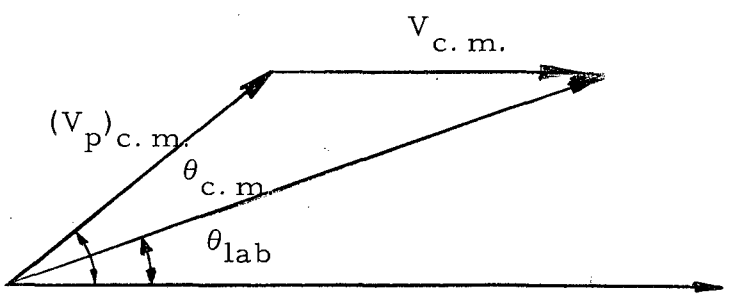

Fig. 10.

If we define

$$x = \frac{V_{c.m.}}{(V_p)_{c.m.}} = \frac{\text{velocity of c.m.}}{\text{velocity of particles in c.m.}} ,$$

then

$$\mu_{lab} = \frac{x + \mu_{c.m.}}{(1+x^2 + 2x\mu_{c.m.})^{1/2}} , \qquad \text{(III.15)}^{\dagger}$$

therefore

$$\frac{d\mu_{c.m.}}{d\mu_{lab}} = \frac{(1+x^2 + 2x\mu_{c.m.})^{3/2}}{1+x\mu_{c.m.}} = \frac{\mu_{lab}(1+x^2 + 2x\mu_{c.m.})}{(1 - \mu_{lab}^2)\, x + \mu_{c.m.}} \qquad \text{(III.16)}$$

and

$$\left(\frac{d\sigma}{d\Omega}\right)_{lab} = \frac{1}{4\pi} \frac{(1+x^2+2x\mu_{c.m.})^{3/2}}{1 + x\mu_{c.m.}} = \frac{1}{4\pi} \frac{\mu_{lab}(1 + x^2 + 2x\mu_{c.m.})}{(1 - \mu_{lab}^2)\, x + \mu_{c.m.}} . \qquad \text{(III.17)}$$

The particular lab angle at which one-half of the protons are ahead and one-half behind is obtained by setting $\mu_{c.m.} = 0$. Then

$$(\mu_{lab})_{1/2} = \frac{x}{(1 + x^2)^{1/2}} \qquad \text{(III.18)}$$

since

$$x = \frac{V_{c.m.}}{(V_p)_{c.m.}} = \frac{1}{4} \frac{V_n}{(V_p)_{c.m.}} = \frac{1}{4} \left[\frac{E_n}{\frac{3}{4}\left(\frac{3}{4} E_n + Q\right)} \right]^{1/2}$$

$$= \left[\frac{E_n}{9E_n + 12Q} \right]^{1/2} = \frac{1}{(3)^{1/2}} \left[\frac{E_n}{3E_n + 4Q} \right]^{1/2} . \qquad \text{(III.19)}$$

Then the average lab proton energy is obtained by averaging the lab proton energy over the lab angular cross section:

$$(\bar{E}_p)_{lab} = \frac{\int (E_p)_{lab} \left(\frac{d\sigma}{d\Omega_{lab}}\right)_{lab} d\Omega_{lab}}{\int \left(\frac{d\sigma}{d\Omega_{lab}}\right)_{lab} d\Omega_{lab}} = \frac{\int (E_p)_{lab} \left(\frac{d\sigma}{d\Omega_{c.m.}}\right)_{c.m.} d\Omega_{c.m.}}{\int \left(\frac{d\sigma}{d\Omega_{c.m.}}\right)_{c.m.} d\Omega_{c.m.}}$$

$$= \frac{1}{2} \int_{-1}^{1} (E_p)_{lab} (\mu_{lab}) \, d\mu_{c.m.}$$

Since

$$V_{c.m.} + (V_p)_{c.m.} \cos\theta_{c.m.} = (V_p)_{lab} \cos\theta_{lab} \qquad \text{(A)}$$

$$(V_p)_{c.m.} \sin\theta_{c.m.} = (V_p)_{lab} \sin\theta_{lab} \qquad \text{(B)}$$

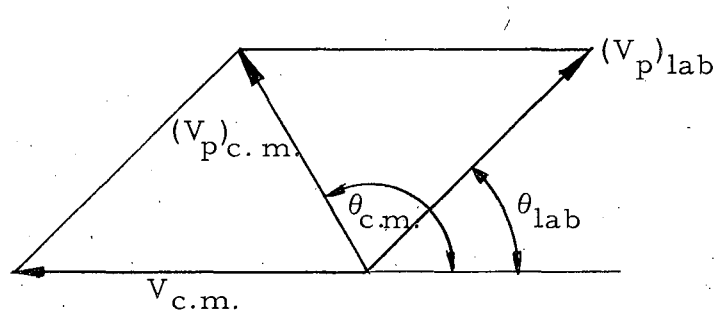

Thus $(A)^2 + (B)^2$ gives

$$(V_p)^2_{lab} = (V_p)^2_{c.m.} + V^2_{c.m.} + 2V_{c.m.} (V_p)_{c.m.} \cos\theta_{c.m.}$$

$$= (V_p)^2_{c.m.} + V^2_{c.m.} + 2V_{c.m.} (V_p)_{c.m.} \mu_{c.m.}$$

or,

$$(E_p)_{lab} (\mu_{c.m.}) = (E_p)_{c.m.} + \frac{E_n}{16} + \frac{1}{2} \left[(E_p)_{c.m.} E_n \mu_{c.m.}\right]^{1/2},$$

therefore

$$(\overline{E}_p)_{lab} = \frac{1}{2} \int_{-1}^{1} \left\{ (E_p)_{c.m.} + \frac{E_n}{16} + \frac{1}{2} \left[(E_p)_{c.m.} E_n \right]^{1/2} \mu_{c.m.} \right\} d\mu_{c.m.}$$

$$= (E_p)_{c.m.} + \frac{E_n}{16} = \frac{3}{4} \left(\frac{3}{4} E_n + Q \right) + \frac{E_n}{16} ,$$

or,

$$(\overline{E}_p)_{lab} = \frac{5}{8} E_n + \frac{3}{4} Q = 0.625 E_n + 0.574 \qquad \text{(III.20)}^{\dagger}$$

The average energy of lab distribution in the plane perpendicular to the counting wire is considered in the following manner.

Consider a particle emitted from the reaction at an angle ϕ_{lab} with the counting wire (see Fig. 11†).

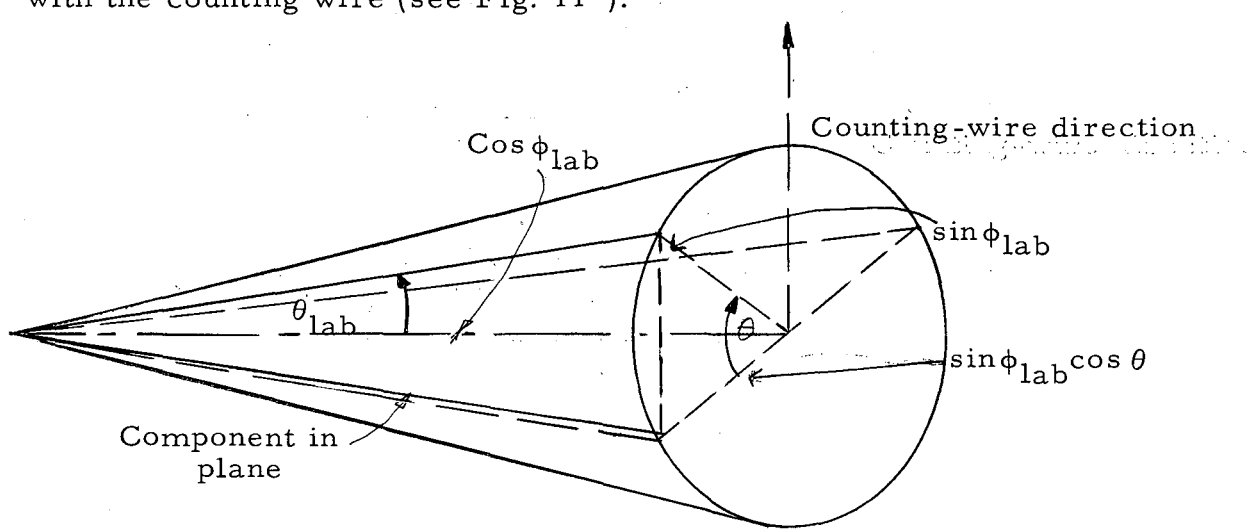

Fig. 11.

The component in the plane is given by

$$(\cos^2 \phi_{lab} + \sin^2 \phi_{lab} \cos^2 \theta)^{1/2} .$$

The average component in the plane perpendicular to the wire is

$$\frac{2}{\pi}\int_0^{\frac{\pi}{2}} [\cos^2\phi_{lab} + \sin^2\phi_{lab}\cos^2\theta]^{1/2}\, d\theta .$$

If we let $K = \sin\phi_{lab}$, the integral becomes a complete elliptical integral of the second kind, and the expression becomes

$$\frac{2}{\pi}\int_0^{\frac{\pi}{2}} (1 - K^2\sin^2\theta)^{1/2} d\theta = \frac{2}{\pi} E(K).$$

At angle ϕ_{lab} the average energy deposited in the plane perpendicular to the counting wire is

$$(\bar{E}_p)_{lab}(\phi_{lab}) = (E_p)_{lab}(\phi_{lab})\ \frac{2}{\pi} E(K) .$$

By integrating this expression over the lab distribution, and defining the results of averaging as $(E_p^{\perp})_{lab}$

$$(E_p^{\perp})_{lab} = \frac{\int (\bar{E}_p)_{lab}(\phi_{lab}) \left(\frac{d\sigma}{d\Omega_{lab}}\right)_{lab} d\Omega_{lab}}{\int \left(\frac{d\sigma}{d\Omega_{lab}}\right)_{lab} d\Omega_{lab}} = \frac{\int (\bar{E}_p)_{lab}(\phi_{lab}) \left(\frac{d\sigma}{d\Omega_{c.m.}}\right)_{c.m.} d\Omega_{c.m.}}{\int \left(\frac{d\sigma}{d\Omega_{c.m.}}\right)_{c.m.} d\Omega_{c.m.}}$$

$$= \frac{1}{2}\int_{-1}^{1} (\bar{E}_p)_{lab}(\phi_{lab})\, d\mu_{c.m.} .$$

Since $\quad (E_p)_{lab}(\mu_{c.m.}) = (E_p)_{c.m.} + \frac{E_n}{16} + \frac{1}{2}(E_p)_{c.m.} E_n \mu_{c.m.}$,

$$(E_p)_{c.m.} = \frac{3}{4}(E_n + Q) \quad \text{and } x = \frac{1}{(3)^{1/2}}\left(\frac{E_n}{3E_n + 4Q}\right)^{1/2} ,$$

therefore

$$(E_p)_{c.m.}(\mu_{c.m.}) = \frac{3}{4}(E_n+Q) + \frac{E_n}{16} + \frac{1}{2}\left(\frac{3}{4}(E_n+Q)E_n\right)^{1/2}\mu_{c.m.}$$

$$= \frac{5}{8}E_n + \frac{3}{4}Q + \frac{E_n}{8x}\mu_c ,$$

and

$$(\bar{E}_p)_{c.m.} = \frac{1}{2}\int_{-1}^{1}\left[\left(\frac{5}{8}E_n + \frac{3}{4}Q\right) + \frac{E_n}{8x}\mu_{c.m.}\right] E(K)d\mu_{c.m.} .$$

Let

$$I_1 = \int_{-1}^{1} E(K)\,d\mu_{c.m.} , \quad I_2 = \int_{-1}^{1} E(K)\,\mu_{c.m.}\,d\mu_{c.m.} .$$

Then

$$(E_p^{\perp})_{lab} = \frac{1}{\pi}\left(\frac{5}{8}E_n + \frac{3}{4}Q\right) I_1(E_n) + \frac{1}{\pi}\frac{E_n}{8x} I_2(E_n)$$

$$= \frac{1}{\pi}\left[I_1(\bar{E}_p)_{lab} + I_2\frac{E_n}{8x}\right] . \qquad \text{(III.21)}^{\dagger}$$

These $I_1(E_n)$ and $I_2(E_n)$, shown graphically in Figs. 12 and 13, have been evaluated by machine computation and hence $(E_p^{\perp})_{lab}$ can be represented approximately as

$$(E_p^{\perp})_{lab} = 0.505\,E_n + 0.450 \qquad \text{(III.22)}^{\dagger}$$

This is shown in Fig. 14, together with lab distribution average energy $(\bar{E}_p)_{lab}$, and energy of the average cosine of the laboratory angle, $(\hat{E}_p)_{lab}$,

where

$$(\hat{E}_p)_{lab} = \frac{E_n}{16}\left\{\overline{\cos\phi}_{lab} + \left[8 + \frac{12Q}{E_n} + (\overline{\cos\phi}_{lab})^2\right]^{1/2}\right\}^2 ,$$

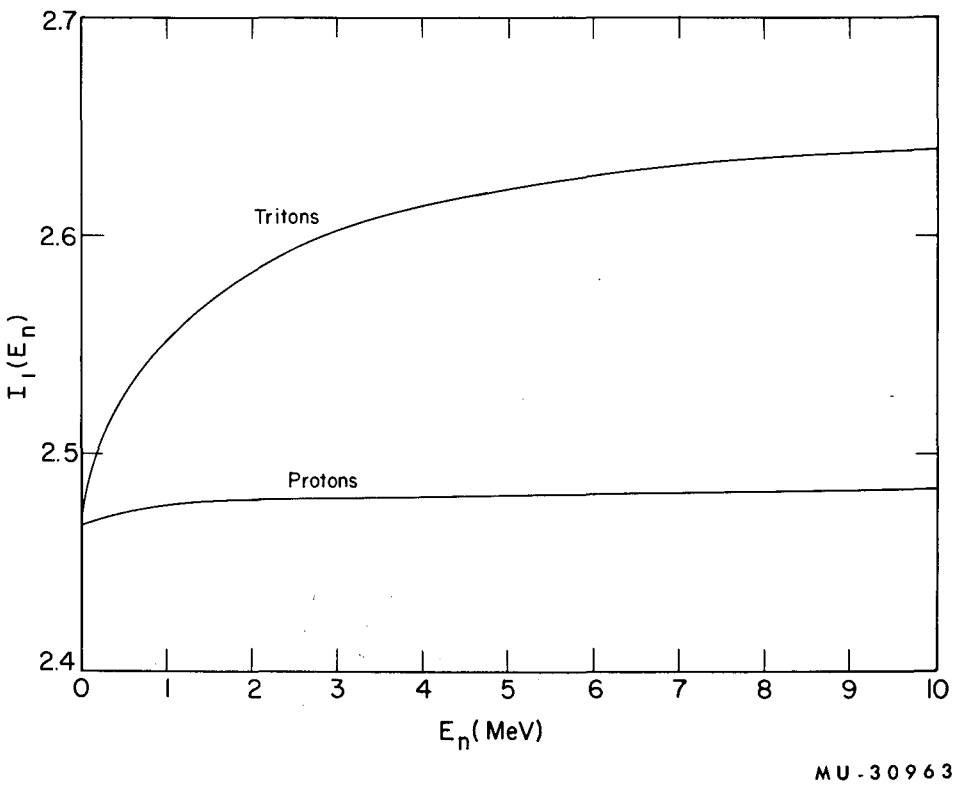

Fig. 12. The energy dependences of $I_1(E_N)$ for protons and tritons.†

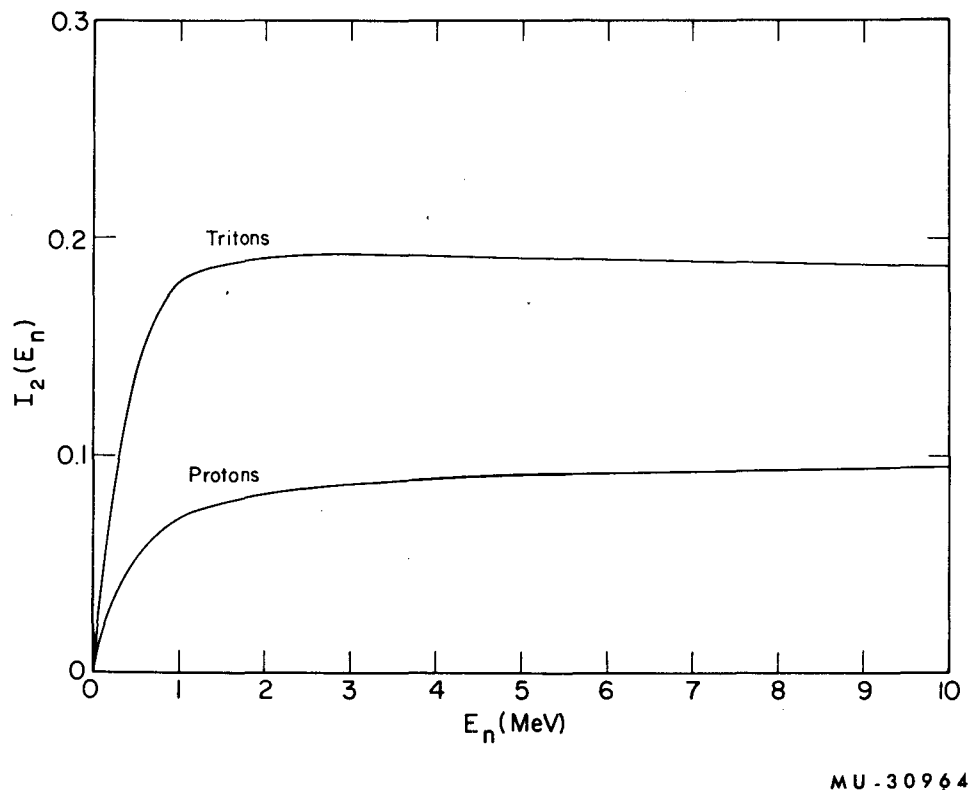

Fig. 13. The energy dependences of $I_2(E_N)$ for protons and tritons.†

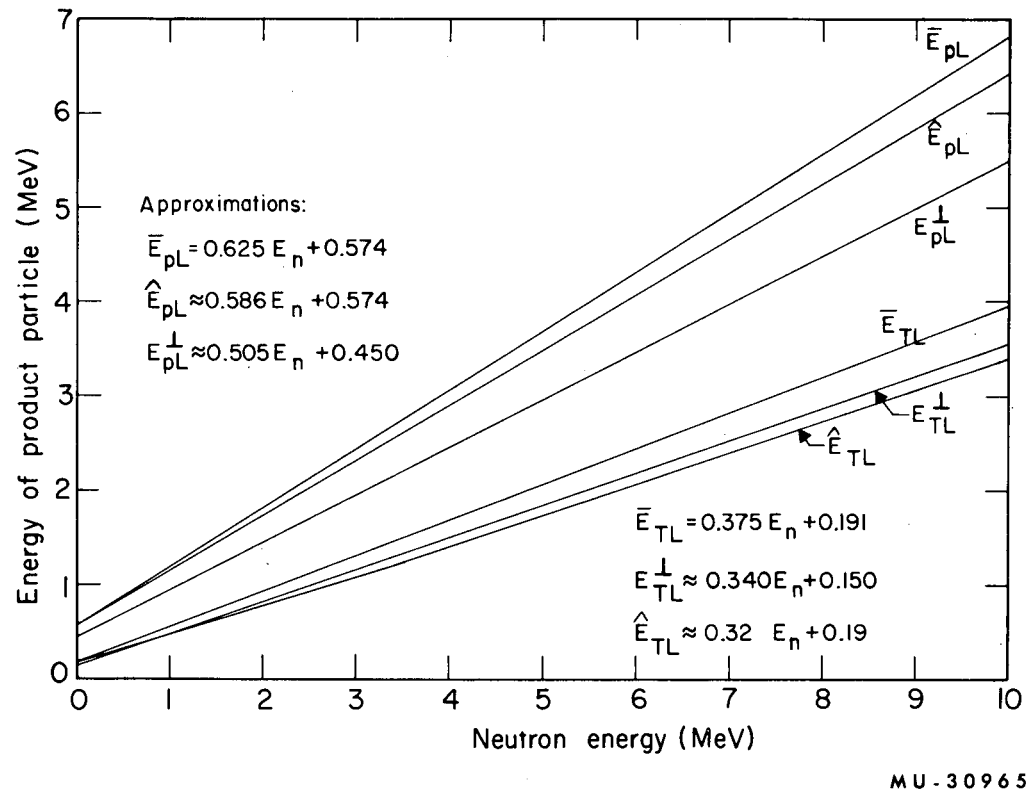

Fig. 14. Energy of $He^3(n, p)T$ products vs neutron energy.

$$\overline{\cos\phi}_{lab} = \bar{\mu}_{lab} = \frac{\int \mu_{lab} \left(\frac{d\sigma}{d\Omega_{lab}}\right)_{lab} d\Omega_{lab}}{\int \left(\frac{d\sigma}{d\Omega_{lab}}\right)_{lab} d\Omega_{lab}} = \frac{1}{2} \int_{-1}^{1} \mu_{lab}\, d\mu_{c.m.}$$

$$= \frac{1}{2} \int_{-1}^{1} \frac{x + \mu_{c.m.}}{(1+x^2+2x\mu_{c.m.})^{1/2}}\, d\mu_{c.m.} = \frac{2}{3}\, x = \frac{2}{3}\, \frac{1}{(3)^{1/2}} \left(\frac{E_n}{3E_n + 4Q}\right)^{1/2}$$

therefore

$$(\hat{E}_p)_{lab} \approx 0.586\, E_n + 0.574. \qquad \text{(III.23)}^{\dagger}$$

For tritons, the same procedures are followed as for protons, and the outlined expressions are:

$$x_T = \frac{V_{c.m.}}{(V_T)_{c.m.}} = (3)^{1/2} \left(\frac{E_n}{3E_n + 4Q}\right)^{1/2} = 3x_p, \qquad \text{(III.24)}$$

$$(\bar{E}_T)_{lab} = \frac{3}{8} E_n + \frac{1}{4} Q = 0.375\, E_n + 0.191\ , \qquad \text{(III.25)}$$

$$(E_T^{\perp})_{lab} = \frac{1}{\pi} \left(\frac{3}{8} E_n + \frac{1}{4} Q\right) I_1(E_n) + \frac{1}{\pi} \left(\frac{3E_n}{8x}\right) I_2(E_n)$$

$$= \frac{1}{\pi} \left[I_1 (\bar{E}_T)_{lab} + I_2 \frac{3E_n}{8x}\right] = 0.340 E_n + 0.15, \qquad \text{(III.26)}^{\dagger}$$

$$(\hat{E}_T)_{lab} = 0.32\, E_n + 0.19. \qquad \text{(III.27)}^{\dagger}$$

These I_1 and I_2 for tritons are depicted in Figs. 12 and 13, respectively. Figure 14 shows plots of $(E_T^{\perp})_{lab}$, $(\bar{E}_T)_{lab}$, and $(\hat{E}_T)_{lab}$.

B. The Probability that Protons or Tritons Will Not Hit the Counter Wall.

There are two different methods for studying this problem.

Method 1.†

Assume that protons are emitted isotropically in the lab system. Then–the proton having been assigned a representative energy depending upon the incoming neutron energy–the problem becomes one of examining the intersection of a sphere, having a radius equal to the track length (range) at this average energy, with the surface of the sensitive volume of the cylindrical counter.

Referring to Fig. 15,† let the reaction occur in region B, at a distance r from the counting wire, and let ℓ be the track length of the proton, for the case $\ell < b$, where b = radius of the detector. Then the normalized spherical surface element is

$$ds = \frac{\ell^2 \sin\theta \, d\theta \, d\phi}{4\pi \ell^2}$$

$$= \frac{d\mu \, d\phi}{4\pi} .$$

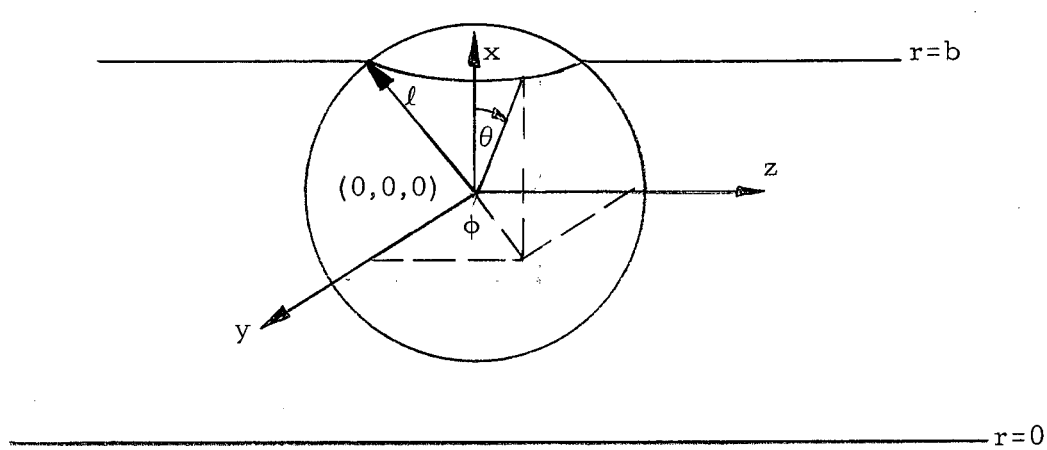

Fig. 15.†

The fractional surface, outside the cylinder, that represents the fractional loss is

$$f(r) = \frac{1}{4\pi} \int_0^{2\pi} \int_1^{\mu(\phi)} d\mu \, d\phi \quad ,$$

where $\mu(\phi)$ represents the line of intersection between the two figures, which can be determined as follows:

Toward the side of the cylinder $(\phi=0)$

$$b^2 = \ell^2 + r^2 + 2r\ell\mu,$$

given

$$\mu_{min} = \frac{b^2 - \ell^2 - r^2}{2r\ell} \quad .$$

An end view is sketched below.

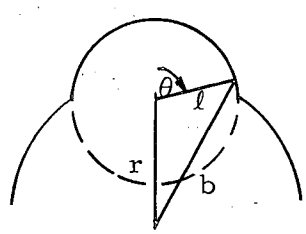

Toward the end of the cylinder $(\phi = \frac{\pi}{2})$

$$\frac{b-r}{\ell} = \cos\theta, \quad \mu_{max} = \frac{b-r}{\ell} \quad .$$

a side view is sketched below.

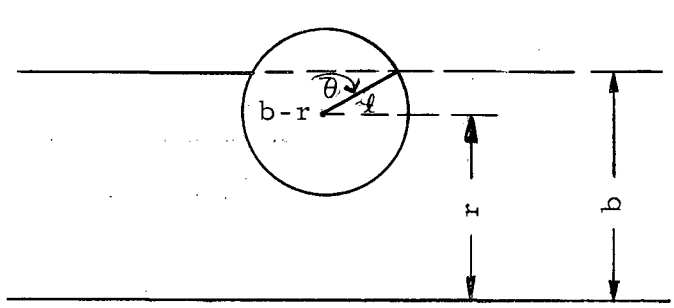

The transition from μ_{min} to μ_{max} along the intersection is approximated:†

$$\mu(\phi) = \frac{b^2 - \ell^2 - r^2}{2r\ell} + \left(\frac{b-r}{\ell} - \frac{b^2-\ell^2-r^2}{2r\ell}\right)\sin^2\phi ,$$

therefore

$$f(r) = \frac{1}{4\pi}\int_0^{2\pi}\int_1^{\mu(\phi)} d\mu d\phi$$

$$= \frac{1}{4\pi}\int_0^{2\pi}\left[\frac{b^2-\ell^2-r^2}{2r\ell} + \left(\frac{b-r}{\ell} - \frac{b^2-\ell^2-r^2}{2r\ell}\right)\sin^2\phi - 1\right] d\phi$$

$$= \frac{1}{4}\left[\left(\frac{b^2-\ell^2}{2\ell}\right)\frac{1}{r} + \left(\frac{b}{\ell} - 2\right) - \left(\frac{3}{2\ell}\right) r\right] ,$$

$$F_{B1} = 1 - f(r) = 1 - \frac{1}{4}\left[\left(\frac{b^2-\ell^2}{2\ell}\right)\frac{1}{r} + \left(\frac{b}{\ell} - 2\right) - \left(\frac{3}{2\ell}\right) r\right] .$$

The volume probability of reaction occurrence at r is

$$g(r)\,dr = \frac{2\pi r dr}{\pi b^2} , \quad \text{therefore} \quad g(r) = \frac{2r}{b^2} .$$

an end view is sketched below.

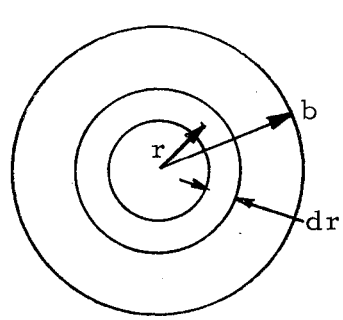

Then the net loss function is

$$L(\ell) = \int_V g(r)\, f(r)\, (r)\, dr.$$

For small spheres no loss is incurred until $r=b-\ell$, at which time the sphere just touches the inside of the cylinder.†

$$L(\ell) = \int_{b-\ell}^{b} \left(\frac{2r}{b^2}\right) \left\{ -\frac{1}{4} \left[\left(\frac{b^2-\ell^2}{2\ell}\right) \frac{1}{r} + \left(\frac{b}{\ell} - 2\right) - \left(\frac{3}{2\ell}\right) r \right] \right\} dr$$

$$= \frac{\ell}{2b}, \qquad 0 \leqslant \ell \leqslant b.$$

This solution can be analytically continued for $\ell > b$ by changing the lower integral limit $(b-\ell)$ to zero; it is then found that†

$$L(\ell) = \frac{1}{4}\left(-\frac{b}{\ell} + \frac{\ell}{b} + 2\right), \qquad b \leqslant \ell \leqslant 2b.$$

The limit on this continuation, $(\ell < 2b)$, is set at the point $\ell = 2b$, where an entirely different geometrical situation exists. The new geometry is essentially that of a small cylinder passing through a large sphere. The only events not hitting the counter wall are those that occur in the small solid angle down the cylinder toward the two ends.

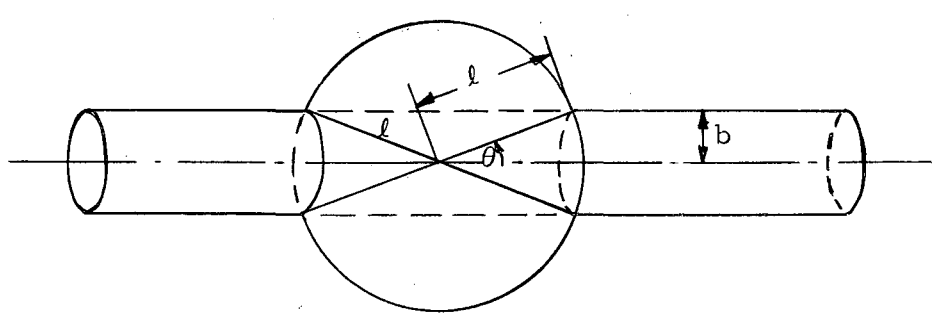

By shifting coordinate systems as shown,

$$ds = \frac{2\pi \ell^2 \sin\theta\, d\theta}{4\pi \ell^2} = -\frac{1}{2}\, d\mu$$

where, now

$$\mu = \cos\theta = \frac{(\ell^2 - b^2)^{1/2}}{\ell} = \left[1 - \left(\frac{b}{\ell}\right)^2\right]^{1/2}.$$

The fractional spherical surface area inside the cylinder is now

$$2\left\{-\frac{1}{2}\int_1^{\left[1-\left(\frac{b}{\ell}\right)^2\right]^{1/2}} d\mu\right\} = 1 - \left[1 - \left(\frac{b}{\ell}\right)^2\right]^{1/2}.$$

However, the above expression was derived for r=0 (axis of the cylinder passing through the center of the sphere). For off-center positions, the area inside the cylinder is greater:

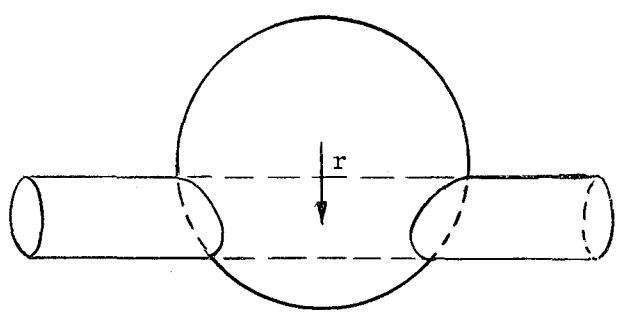

This can be taken into account by a weighting function w(r). It was decided to match this function to the geometry at $\ell = 2b$:

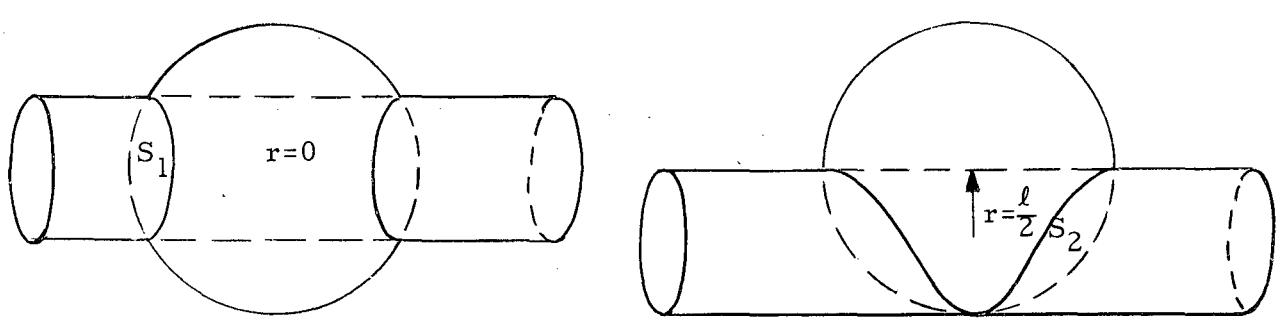

The function w(r) is adjusted so that as r goes from zero to one-half, w(r) goes from S_1 to S_2. A linear weighting function was chosen, and the condition was found to be satisfied by

$$w(r) = \frac{(S_2/S_1 - 1)}{\frac{\ell}{2}} r + 1.$$

The ratio of the area was estimated to be

$$\frac{S_2}{S_1} \approx 1.294,$$

so that then the weighting function became

$$w(r) = 1 + 0.588 \frac{r}{\ell} .$$

Thus, the fractional net loss due to the hitting of the wall is

$$\left\{1 - [1 - (\frac{b}{\ell})^2]^{1/2}\right\} (1 + 0.588 \frac{r}{\ell}) .$$

This quantity was multiplied by a factor to compensate for the angular distribution. Assuming that neutrons are introduced into the counter from the side (perpendicular to the counting wire), the relative angular cross section must be estimated in the direction of the ends. The angular cross sections have been derived in the treatment of the proton energy distribution:

$$\left(\frac{d\sigma}{d\Omega}\right)_{lab} = \frac{1}{4\pi} \frac{\mu_{lab}(1+x^2+2x\mu_{c.m.})}{(1-\mu^2_{c.m.})x+\mu_{c.m.}} ,$$

as the angle approaches 90 deg, $\mu_{lab} \rightarrow 0$, and the denominator approaches the quantity $x+\mu_{c.m.}$. By substituting in the expression

$$x+\mu_{c.m.} = \mu_{lab}(1+x^2+2x\mu_{c.m.})^{1/2},$$

we obtain from the relationship between the angles in the lab and c.m. system

$$\left(\frac{d\sigma}{d\Omega_{lab}}\right)_{lab} \rightarrow \frac{1}{4\pi}\ (1+x^2+2x\mu_{c.m.})^{1/2} \ .$$

Based on the fact that when $\mu_{lab}=0$ then $\mu_{c.m.}=-x$,

$$\left(\frac{d\sigma}{d\Omega}\right)_{lab} = \frac{1}{4\pi}\ (1-x^2)^{1/2}.$$

The above expression is the probability per unit solid angle that protons will leave the reaction site in a direction perpendicular to that of the incoming neutron. The relative probability is

$$\left(\frac{d\sigma}{d\Omega}\right)_{lab} = (1-x^2)^{1/2},$$

and the fractional probability of not hitting the counter wall becomes

$$(1-x^2)^{1/2}\left\{1-[1-(\frac{b}{\ell})^2]^{1/2}\right\}[1+0.588\,\frac{r}{\ell}]$$

the fractional loss at point r is one minus this quantity:

$$f(r) = 1-(1-x^2)^{1/2}\left\{1-[1-(\frac{b}{\ell})^2]^{1/2}\right\}[1+0.588\,\frac{r}{\ell}].$$

Again, this must be integrated over the counter volume to obtain the net loss, or the probability that protons will hit the counter wall is:

$$L(\ell) = \frac{2}{b^2}\int_0^b \left\{1-(1-x^2)^{1/2}[1-(1-(\frac{b}{\ell})^2)^{1/2}]\ (1+0.588\,\frac{r}{\ell})\right\} rdr\ ,$$

therefore

$$L(\ell) = 1-(1-x^2)^{1/2}[1-(1-(\frac{b}{\ell})^2)^{1/2}](1+0.392\,\frac{b}{\ell})\ .$$

Then the probability that protons will not hit the counter wall is:

$$f_1 = 1-L(\ell) = (1-x^2)^{1/2}[1-(1-(\frac{b}{\ell})^2)^{1/2}](1+0.392\,\frac{b}{\ell})\ . \quad \text{(III.28)}$$

Because the track length ℓ is related to the initial energy of the ionizing particle through the range-energy relationships, the f_1 becomes a function of energy and differs for each type of particle. In the case of the proton from the $He^3(n,p)T$ reaction, the energy assigned to the isotropic distribution in this method is the energy corresponding to the average cosine of the proton angle. From Subsec. III.A,

$$(\hat{E}_p)_{lab} = \frac{E_n}{16}\left[\bar{\mu}_{lab} + \left(8 + \frac{12Q_{np}}{E_n} + \bar{\mu}_{lab}^2\right)^{1/2}\right]^2 .$$

This was selected to account for the forwardness of the angular distribution.

Method 2.†

This approach treated the case of a single track. The treatment assumed that the important quantity is the track component perpendicular to the counting wire, because the parallel component passes down the length of the counter.

Consider an ionization track of length ℓ lying in a plane perpendicular to the counting wire. The origin of the track may occur with equal probability at any point inside a circle of radius b formed by the counter. The figure below shows that a track in a given direction will deposit all its energy if it is to the left of the circle of radius b whose center is located a distance ℓ back from the counting wire.

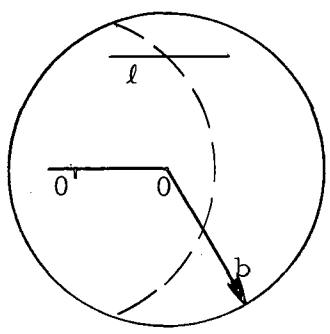

The fraction depositing all their energy will be proportional to the relative area bounded by the intersection of the two circles: The expression for this area is

$$f_{p1}(E_n) = 1 - \frac{2}{\pi}\left[\left(\frac{\ell}{2b}\right)\left(1-\left(\frac{\ell}{2b}\right)^2\right)^{1/2} + \sin^{-1}\left(\frac{\ell}{2b}\right)\right] . \qquad \text{(III.29)}$$

For a small track length ℓ, this expression becomes

$$f_{p1}(E_n) = 1 - \frac{4}{\pi}\left(\frac{\ell}{2b}\right), \qquad \text{(III.30)}$$

which is similar to the expression found for the intersection of small spheres with large cylinders. Since particles from a reaction are emitted in a distribution that varies in angle and energy, the important quantity is then the average of the lab distribution in the plane perpendicular to the counting wire. This quantity has already been calculated for each of the various particles. Representative energies are used to compute the track lengths to evaluate the function f_1, given above.

C. Consideration of Two Simultaneously Emitted Protons and Tritons

At neutron energies below E_{crit}* the probability of not hitting the wall for a proton and a triton, respectively, based on the preceding section may be taken as

$$f_{p1}(E_n) = 1 - \frac{2}{\pi}\left\{\frac{\ell_p}{2b}\left[1-\left(\frac{\ell_p}{2b}\right)^2\right]^{1/2} + \sin^{-1}\left(\frac{\ell_p}{2b}\right)\right\} , \qquad \text{(III.29a)}$$

$$f_{T1}(E_n) = 1 - \frac{4}{\pi}\left(\frac{\ell_T}{2b}\right) . \qquad \text{(III.30a)}$$

Therefore the net probability of not hitting the wall is a combination of these functions.

From Subsec. III.A we see that the angular distribution for a proton may be approximated isotropically in the lab system, while for the case of a triton it tends to be distributed more forward. If the distribution with the forward track component is considered, it can be seen that the degree of isotropy must be determined. Because the

---

* E_{crit} is defined in Appendix A.

representative angle of the distribution increases from zero, the trend toward isotropy moves relatively. Let

$$\overline{\phi}_{lab} = \cos^{-1}\overline{\mu}_{c.m.}$$

in the following illustration:

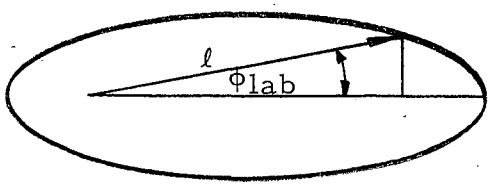

The degree of isotropy may be indicated by the value of $\sin\overline{\phi}_{lab}$ as an approximation to the physical situation.

Therefore the combined probability of not hitting the wall is

$$f_1(E_n) = f_{p1} \cdot f_{T1}^{\sin\overline{\phi}_{lab}}$$

$$= \left(1 - \frac{2}{\pi}\left\{\frac{\ell_p}{2b}\left[1 - \left(\frac{\ell_p}{2b}\right)^2\right]^{1/2} + \sin^{-1}\left(\frac{\ell_p}{2b}\right)\right\}\right)\left[1 - \frac{4}{\pi}\left(\frac{\ell_T}{2b}\right)\right]^{(1-\overline{\mu}_T^2)^{1/2}} \qquad \text{(III.31)}^{\dagger}$$

For neutron energy $E_n \geq E_{crit}$, then [c.f. (III.28)],

$$f_1(E_n) = \left\{(1-x_p^2)^{1/2}\left[1 - \left\{1 - \left(\frac{b}{\ell_p}\right)^2\right\}^{1/2}\right]\left(1 + 0.392\,\frac{b}{\ell_p}\right)\right\}\left[1 - \frac{4}{\pi}\left(\frac{\ell_T}{2b}\right)\right]^{(1-\overline{\mu}_T^2)^{1/2}} \qquad \text{(III.32)}$$

D. Unfolding of the Wall Effect of Protons and Tritons

The wall effect due to recoil protons and tritons from any neutron energy will contribute counts of all energies below that energy. Therefore the raw spectrum recorded from the He^3 neutron detector will include the above wall effects.

The counts at any channel include the events of protons, tritons, recoiled helium nuclei, deuterons, and their wall effects. This makes the unfolding of wall effects very complicated. However, the fact that

the recorded spectrum at top channel represents only "full size" (n, p) events simplifies the analysis, because all other nuclear reactions can only contribute counts at lower energies.

Starting from the top channel of the raw spectrum, let the counts recorded there be C_N.

Since the probability, for protons and tritons, of not hitting the wall is $f_1(E_N)$, then the true events are

$$\frac{C_N}{f_1(E_N)} .$$

Therefore the number of counts contributing to lower energies is:

$$\frac{C_N}{f_1(E_N)} - C_N = \frac{C_N}{f_1(E_N)} [1 - f_1(E_N)] .$$

In general, at any channel E_i, the counts there due to the contribution of the wall effect from (n, p) events with energy larger than E_i is then

$$\int_{E_i}^{E_N} \frac{C_N(E)}{f_1(E)} [1 - f_1(E)] \, P(E \rightarrow E_i) \, dE ,$$

where

$P(E \rightarrow E_i)$ = the probability per unit energy that the (n, p) event products (proton and triton) of energy E deposit only E_i inside the sensitive volume due to the wall effect

$$= \left[\frac{1}{E_b^2 E_i^2} (E_b E^2 - \frac{2}{3} E^3) + \frac{E^2}{2E_L E_i^2} + \frac{1}{2E_L} \right] ,$$

$C_N(E)$ = counts of raw (n, p) spectrum at channel E,

or $$C_p(i) = \int_{E_i}^{E_N} \frac{C_N(E)}{f_1(E)} [1 - f_1(E)] \, P(E \rightarrow E_i) dE \qquad \text{(III.33)}$$

This $C_p(i)$ should be calculated for i running from i = N-1 to i = 0 for a fixed top channel as an upper limit. This calculated result

is then subtracted from the original raw (n, p) spectrum, which is the result of unfolding deuteron and recoil effects, at the corresponding channel; the difference serves as a new spectrum for the next calculation. The next calculation is made by changing E_N to E_{N-1} and computing $C_p(i)$ for $i = N-2$ to $i = 0$, etc. These processes are repeated until the upper limit of the integration reaches the lower limit of the original raw spectrum..

IV. RECOIL EFFECT

A.† Recoil Cross Sections

The recoil effect in the detector arises when a He^3 nucleus passes out of the sensitive volume of the detector. This He^3 nucleus comes from the elastic scattering reactions $He^3(n, n)He^3$. The total elastic scattering cross section of He^3 was obtained through the comparison of the partial cross sections with the total cross-section, and by numerical integration of the differential elastic scattering cross sections:

$$\sigma_S(E_n) = \frac{1}{4\pi} \int \left(\frac{d\sigma}{d\Omega}\right) d\Omega = \frac{1}{2} \int_{-1}^{1} \frac{d\sigma}{d\Omega} (E_n, \mu)\, d\mu \, .$$

The elastic scattering cross section for zero neutron energy was calculated from potential scattering to be

$$\sigma_S(0) = 4\pi R^2 = 4\pi (1.5 \times 10^{-13} A^{1/3})^2 = 0.588\text{b}.$$

Experimental data on the He^3 differential elastic scattering cross section are available. Because there are some contradictions among them, it is necessary to reconcile the values from the different sources. This was done by plotting smooth curves of differential cross sections as functions of neutron energy. The point for zero-energy neutrons was taken as

$$\frac{d\sigma}{d\Omega}(0,\mu) = \frac{\sigma_S(0)}{4\pi} = 46.8 \text{ mb}.$$

These curves are shown in Figs. 16, 17, 18, and 19.

For the convenience of computer calculations, it is found desirable to express this differential cross section through an analytical approximation, as an expansion of Legendre polynomials:

$$\frac{d\sigma(E_n, \mu)}{d\Omega} = \sum_{\ell=0}^{3} a_\ell(E_n) P_\ell(\mu). \qquad \text{(IV.1)}$$

The energy-dependent coefficients $a_\ell(E_n)$ were determined by

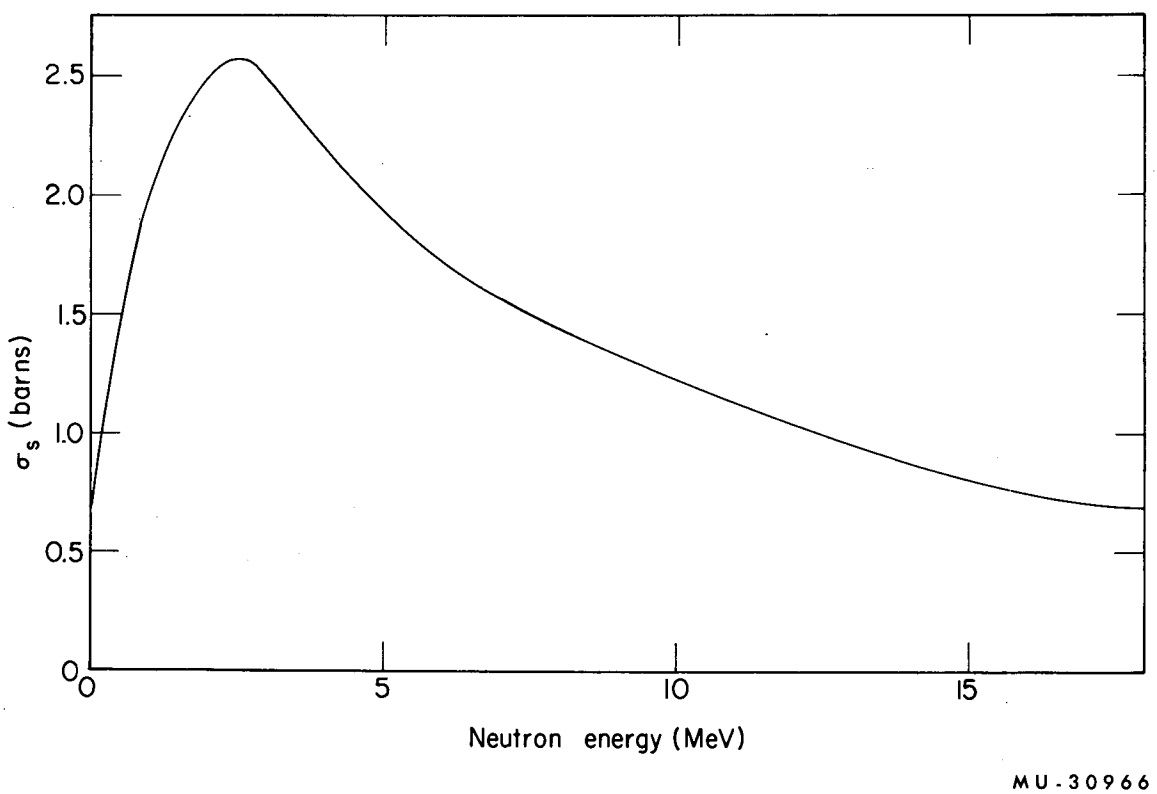

Fig. 16. Total elastic scattering cross section of $He^3(n, n)He^3$ vs neutron energy.

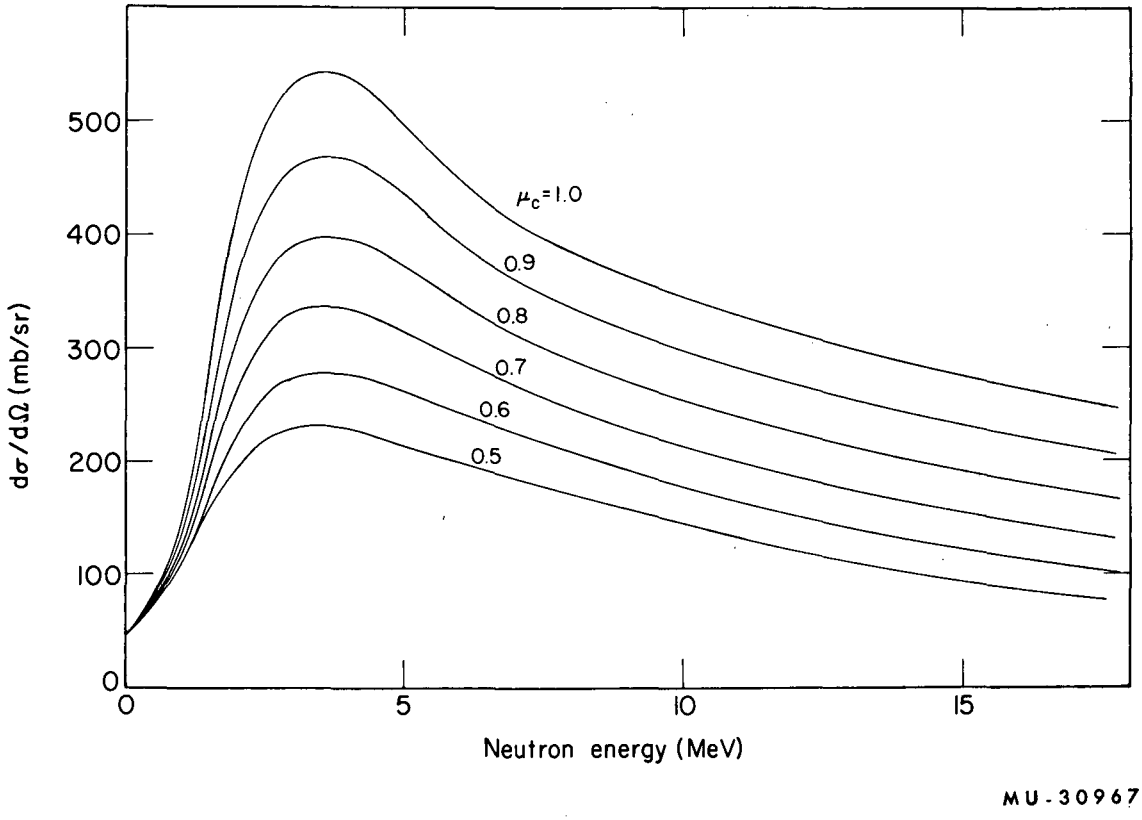

Fig. 17. Differential scattering cross section of $He^3(n, n)He^3$ (μ_c from 0.5 to 1).

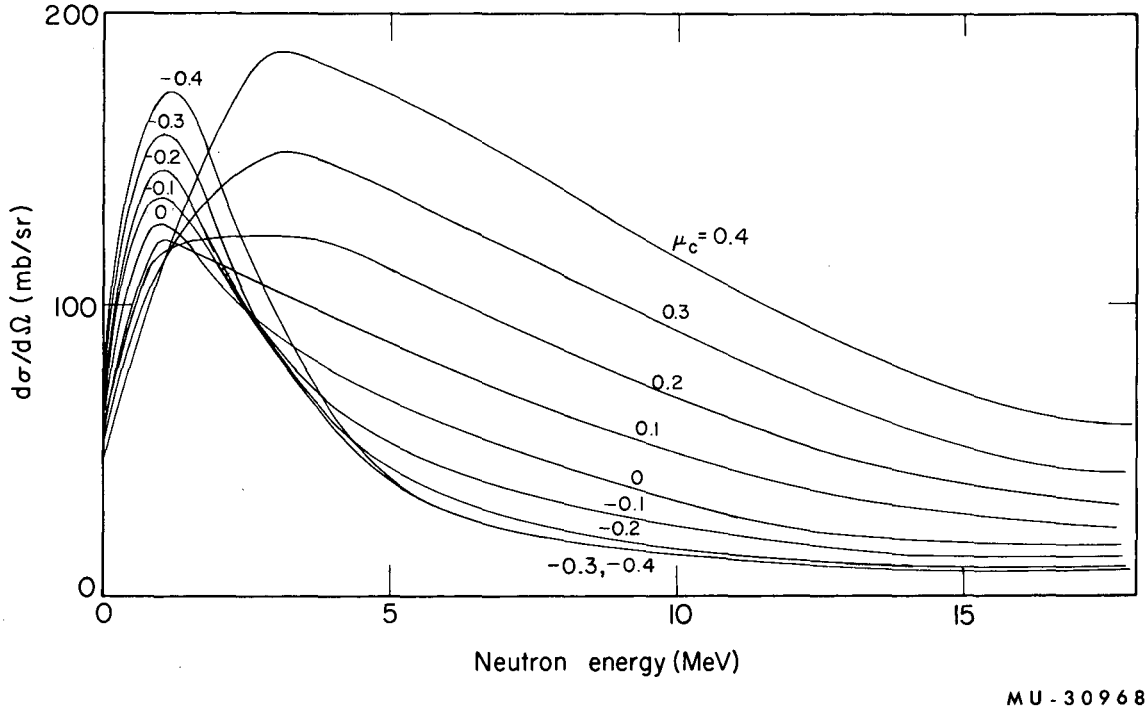

Fig. 18. Differential scattering cross section of $He^3(n, n)He^3$ (μ_c from -0.4 to 0.4).

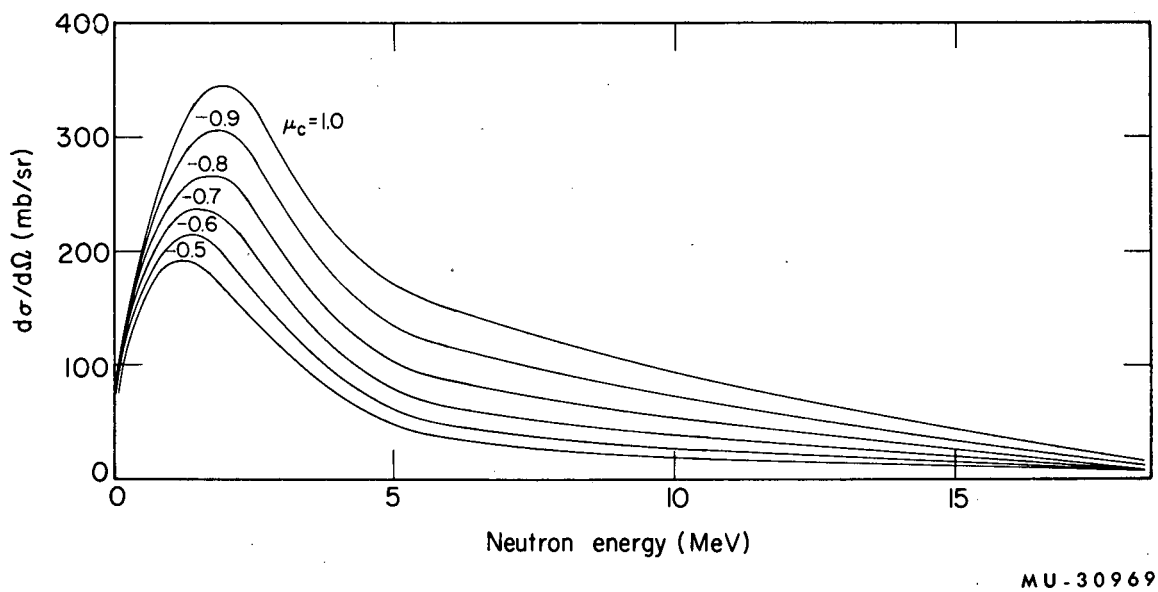

Fig. 19. Differential scattering cross section of $He^3(n, n)He^3$ (μ_c from -0.5 to -1).

least-square fitting of the plots of

$$\frac{d\sigma(E_n, \mu)}{d\Omega} \text{ vs } E_n$$

at a sufficient numer of energies. The fits were checked to verify that $\sigma_S(E_n) = 4\pi\, a_0(E_n)$. Curves of the coefficients $a_\ell(E_n)$ vs E_n are shown in Fig. 20.

B.† Energy of Recoiled Nuclei

The energy of the recoiled He^3 nuclei can be obtained by using the conservation of both energy and momentum, as

$$\frac{E_r}{E_n} = \frac{3}{8}(1 - \mu_{c.m.}) , \qquad \text{(IV.2)}$$

where

E_r = energy of He^3 nucleus after scattering in the lab system,

E_n = incident neutron energy in the lab system,

$\mu_{c.m.}$ = cosine of scattering angle of neutron in the c.m. system.

It is seen from Subsec. IV.B. that the recoil energy E_r depends on both the incident energy and the scattering angle of the neutrons. This E_r ranges from a maximum value of $3/4\ E_n$(at $\mu_{c.m.} = -1$) to zero (at $\mu_{c.m.} = 1$). This fact will be considered in the unfolding of recoil effects.

The average energy of the recoiling He^3 ion in the lab system in a plane perpendicular to the counting wire is obtained through a similar consideration to that of protons in Subsec. III.A, as

$$\bar{E}_{He} = \frac{3E_n}{8\pi} \left(\frac{8}{3} - I_2\right) , \qquad \text{(IV.3)}$$

where

$$I_2 = \int_{-1}^{1} \mu_{c.m.} \Xi(\mu_{c.m.})\, d\mu_{c.m.} ,$$

and

$$\Xi(\mu_{c.m.}) = \int_0^{\frac{\pi}{2}} (1 - K^2 \sin^2\theta)^{1/2}\, d\theta$$

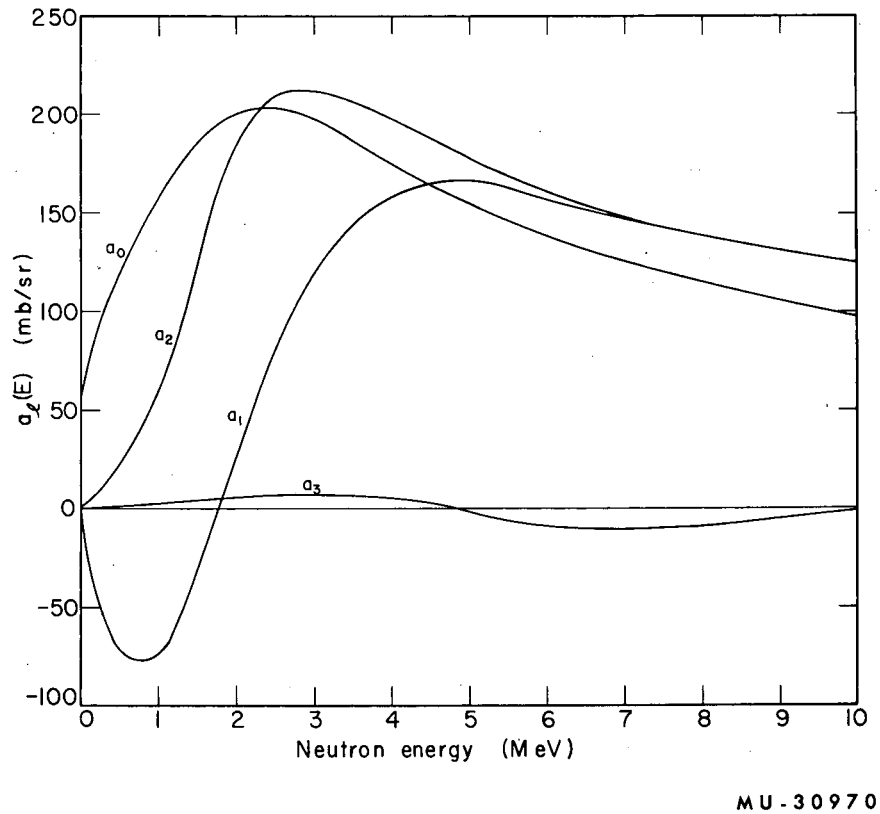

Fig. 20. Legendre polynomial expansion coefficients.

is the complete elliptical of the second kind, and

$$K = \left(1 - \frac{4E_r}{3E_n}\right)^{1/2} = [1 - \frac{1}{2}(1 - \mu_{c.m.})]^{1/2}.$$

For the head-on collision

$$E_{He} = \frac{3}{4} E_n. \qquad \text{(IV.4)}$$

C. The Probability, $P(E_r)$, per Unit Energy that a Neutron of Energy E Undergoing the Reaction $He^3(n, n)He^3$ Will Cause that Helium-3 Nucleus to Recoil with Energy E_r

The probability per unit angle of a scattered neutron scattering at an angle $\theta_{c.m.}$ (in the c.m. system) is

$$p(\theta_{c.m.}) = C\frac{d\sigma}{d\theta} = C\frac{d\sigma}{d\Omega} \cdot \frac{d\Omega}{d\theta} = C\,2\pi \sin\theta_{c.m.}\left(\frac{d\sigma}{d\Omega}\right)_{c.m.},$$

where C is a constant to be determined later.

The probability per unit energy that this scattering will result in a recoiling nucleus of energy E_r is

$$p(E_r)\,dE_r = p(\theta_{c.m.})\,d\theta_{c.m.} = p(\theta_{c.m.})\frac{d\theta_c}{dE_r}\,dE_r.$$

Where C and E_r are related by Eq. (IV.2), i.e.,

$$\frac{E_r}{E} = \frac{3}{8}(1 - \cos\theta_{c.m.}),$$

then

$$\frac{dE_r}{d\theta_{c.m.}} = \frac{3}{8} E \sin\theta_{c.m.},$$

and

$$p(E_r) = C\frac{16\pi}{3E}\left(\frac{d\sigma}{d\Omega}\right)_c.$$

To normalize this expression,

$$1 = \int_0^{E_{max}} p(E_r)\, dE_r = C \frac{16\pi}{3E} \int_0^{E_{max}} \left(\frac{d\sigma}{d\Omega}\right)_c dE_r$$

$$= C \int_0^{E_{max}} \left(\frac{d\sigma}{d\Omega}\right)_{c.m.} 2\pi \sin\theta_{c.m.}\, d\theta_{c.m.}$$

$$= C \int_\Omega \left(\frac{d\sigma}{d\Omega}\right)_{c.m.} d\Omega_{c.m.} = C\sigma_S ,$$

therefore

$$C = \frac{1}{\sigma_S}$$

and

$$p(E_r) = \frac{16\pi}{3E} \frac{1}{\sigma_S} \left(\frac{d\sigma}{d\Omega}\right)_{c.m.}$$

$$= \frac{16\pi}{3E} \frac{1}{\sigma_S} \sum_{\ell=0}^{3} a_\ell P_\ell(\mu)$$

$$= \frac{16\pi}{3E} \frac{1}{\sigma_S} \sum_{\ell=0}^{3} a_\ell P_\ell\left(1 - \frac{8}{3}\frac{E_r}{E}\right). \qquad \text{(IV.5)}$$

D. Unfolding of Recoil Effects

The unfolding of recoil effects of the spectra recorded is a very important process to increase the useful energy range of a He^3 gas-filled detector because of the fact that neutrons in excess of 1 MeV are able to cause He^3 nuclei to recoil with sufficient energy to overlap the low-energy part of the spectrum due to the (n, p) events. According to Subsec. IV. B, neutrons with an energy of 1 MeV can cause a He^3 nucleus

of 0.75 MeV. This is close to 0.764 MeV, which comes from the products of an (n, p) event. Furthermore, the wall effect on the He^3 nucleus track will cause counts at lower energies. Therefore the unfolding of the recoil effect will consist of two main parts, discussed below:

Part 1: The tracks of He^3 nuclei that do not intersect the counter wall,

Part 2: The tracks of He^3 nuclei that do intersect the counter wall.

The analysis is then based on the following assumptions:

(a) The nuclear reaction site density is constant throughout the volume.

(b) The nuclei produce tracks along which the specific ionization is constant; i. e., the pulse height is produced proportionally to the length of the track falling inside the sensitive volume. This assumption follows from the assumption c of Subsec. II.A. Since the energy-range relation for a He^3 nucleus in He^3 is calculated by aid of proton curves.

Part 1: The tracks of He^3 nuclei do not intersect the counter wall; i. e., the He^3 nuclei will deposit their whole energy inside the sensitive volume.

Suppose a recorded spectrum is given; then let

C_N = top channel counts recorded solely from (n, p) events,

$f_1(E_N)$ = total fraction, or the probability that protons will not hit the counter wall,

Then

$$\frac{C_N}{f_1(E_N)}$$

is the true number of (n, p) events that actually happen in the sensitive volume.

The number of scattering events corresponding to the number of (n, p) events can be closely approximated by

$$\frac{\sigma_S(E_N)\, C_N}{\sigma_{n,p}(E_N)\, f_1(E_N)}$$

These recoil helium nuclei can then cause counts at energies below $3/4\ E_N$.

If only those events that do not hit the detector wall are considered, letting the probability per unit energy of a recoil nucleus reaching E_r be $p(E_r)$, then the number of counts in channel i coming from the top channel N is

$$C_{He^3}(N \rightarrow i) = \frac{C_N \, \sigma_S(E_N) \, f_2(E_N)}{\sigma_{n,p}(E_N) \, f_1(E_N)} \, p(E_i) \, \Delta i E,$$

$$E_i < \frac{3}{4} E_N \, , \qquad E_N > E_r > E_i,$$

where $\Delta_i E$ = energy width of channel i

$f_2(E_N)$ = probability of a scattering event for which a nucleus of energy E_N will not hit the wall.

In general, at any other channel j below N

$$C_{He^3}(j \rightarrow i) = \frac{C_j \, \sigma_S(E_j) \, f_2(E_j)}{\sigma_{n,p}(E_j) \, f_1(E_j)} \, p(E_i) \, \Delta_i E$$

for all channels i where, from Subsec. III.B, Eq. III.30, this $f_2(E_n)$ may be taken as

$$f_2(E_n) = 1 - \frac{4}{\pi}\left(\frac{\ell_{He}}{2b}\right) \quad . \tag{IV.6}$$

Part 2: The tracks of He^3 nuclei do intersect the counter wall; i.e., the He^3 nuclei will deposit only part of their energy (due to the wall effect) inside the sensitive volume. These events can be analyzed as follows.

Let $f_3(E_N)$ be the probability, per unit energy at neutron energy E_N for a scattering event, at which the recoil nucleus will hit the wall. This equals $1 - f_2(E_N)$, [where $f_2(E)$ is defined as before].

Also let $P(E \rightarrow E_i)$ be the probability per unit energy that a recoiling nucleus of energy E deposits only energy E_i inside the sensitive volume due to the wall effect.

Since the number of counts in channel i, due to wall effect, can come from all the track energies between the limits E_i and $3/4 \, E_N$, the number of counts due to partial deposition of energy is

$$C_{(He^3)_2} = \int_{E_i}^{3/4\,E_N} \frac{C_N \sigma_S(E_N) f_3(E_N)}{\sigma_{n,p}(E_N) f_1(E_N)} P(E)\, P(E \to E_i) \Delta_i E dE.$$

In general, at any other channel j below N the contribution of the partial deposition of energy in counts is expressed as

$$C_{(He^3)_2} = \int_{E_i}^{3/4\,E_j} \frac{C_j \sigma_S(E_j) f_3(E_j)}{\sigma_{n,p}(E_j) f_1(E_j)} p(E) P(E \to E_i) \Delta_i E dE$$

$$= C_j \frac{\sigma_S(E_j) f_3(E_j)}{\sigma_{n,p}(E_j) f_1(E_j)} \Delta_i E \int_{E_i}^{3/4\,E_j} p(E) P(E \to E_i) dE,$$

$$E_i \leqslant E \leqslant \frac{3}{4} E_j.$$

Therefore the total counts due to recoil helium nuclei is the sum of these two parts; i. e. ,

$$C_{He^3}(j \to i) = \frac{C_j \sigma_S(E_j) f_2(E_j)}{\sigma_{n,p}(E_j) f_1(E_j)} p(E_i)\, \Delta_i E$$

$$+ \frac{C_j \sigma_S(E_j) f_3(E_j)}{\sigma_{n,p}(E_j) f_1(E_j)} \int_{E_i}^{3/4\,E_j} p(E)\, P(E \to E_i)\, dE\, \Delta_i E$$

$$= \frac{C_j \sigma_S(E_j)}{\sigma_{n,p}(E_j) f_1(E_j)} \left[f_2(E_j)\, p(E_i) + f_3(E_j) \int_{E_i}^{3/4\,E_j} p(E) P(E \to E_i) dE \right] \Delta_i E. \tag{IV.7}$$

This quantity $C_{He^3}(j \rightarrow i)$ should be first calculated for each i running from $i = 3/4\ N$ down to $i = 0$ for a fixed upper limit $j = N$. The results are then subtracted from the corresponding counts of the raw spectrum. These differences serve as a new spectrum for the next calculation. The next calculation is made by changing E_j to E_{j-1}, and letting i run from $i = (3\,N/4) - 1$ to $i = 0$, etc. These processes are repeated until the upper limit of the calculation reaches the channel equivalent to a neutron energy of 1 MeV. At 1 MeV the energies of recoil He^3 nuclei begin to overlap the energies of events from n,p reactions

V. EFFECT OF THE REACTION $He^3(n,d)D$

A. Reaction Energy†

The endothermic reaction

$$ {}_2He^3 + {}_0n^1 = {}_1D^2 + {}_1d^2 + Q_{n,d} \tag{V.1} $$

has a reaction energy

$$ Q_{n,d} = -3.27 \text{ MeV}. \tag{V.2} $$

The threshold for the occurrence of this reaction is then

$$ E_{th} = 4/3\ Q_{n,d} = 4.36 \text{ MeV}. $$

Therefore, at energies above threshold, the total energy carried away by the two deuterons is

$$ E_n + Q_{n,d}. \tag{V.3} $$

From considerations similar to those in Subsec. III. A, the energy of either deuteron in the lab system is

$$ (E_D)_{lab} = \frac{E_n}{8}\left[\cos\phi_{lab} + (2 + \frac{4Q_{n,d}}{E_n} + \cos^2\phi_{lab})^{1/2}\right]^2. \tag{V.4} $$

At threshold, the $\cos\phi_{lab} = 1$, and

$$ (E_D)_{lab} = \frac{Q_{n,d}}{6} \quad . \tag{V.5} $$

Both particles go straight forward together.

At any energy above threshold, the angles in the c. m. and lab systems are related (see Subsec. III.A) by

$$ \mu_{lab} = \frac{x + \mu_{c.m.}}{(1 + x^2 + 2x\mu_{c.m.})^{1/2}} \tag{V.6} $$

where

$$ x = \frac{V_{c.m.}}{(V_D)_{c.m.}} = \left(\frac{E_n}{3E_n + 4Q_{n,d}}\right)^{1/2} \tag{V.7} $$

and the angular cross section is given by

$$\left(\frac{d\sigma}{d\Omega}\right)_{lab} = \frac{1}{4\pi}\frac{\mu_{lab}(1+x^2+2x\mu_{c.m.})}{(1-\mu_{lab}^2)x+\mu_{c.m.}} \quad . \tag{V.8}$$

From these relations it is found that

$$\mu_{lab,1/2} = \frac{x}{(1+x^2)^{1/2}} \quad , \tag{V.9}$$

$$(\overline{E}_D)_{lab} = \frac{E_n + Q_{n,d}}{2} \quad , \tag{V.10}$$

$$\text{fraction forward} = \frac{1+x}{2} \quad . \tag{V.11}$$

From Eq. (V.4) let $\phi_{lab} = 180$ deg, then

$$2 + \frac{2Q_{n,d}}{E_n} + 1 < 1, \text{ for } E_n < |2Q_{n,d}|,$$

then $$(E_D)_{lab} < 0.$$

This means that there are no deuterons coming off in a backward direction. Therefore, below this critical energy, the velocity of the deuterons in the c.m. system in the backward direction is less than the velocity of the center of mass. And at $E_n = 2|Q_{n,d}|$, from Eq. V.7, $x = 1$; for $4/3\,|Q_{n,d}| < E_n < 2Q_{n,d}$, $x > 1$. Then the reevaluation of $\overline{\mu}_{lab}$ gives

$$\overline{\mu}_{lab} = \frac{2}{3}x \quad \text{for } 2\,|Q_{n,d}| \leq E_n < \infty \tag{V.12}$$

$$= 1 - \frac{1}{3x^2} \quad \text{for } \frac{4}{3}\,|Q_{n,d}| \leq E_n \leq 2Q_{n,d}. \tag{V.13}$$

The average energy of the distribution in a plane perpendicular to the counting wire is calculated, similar to that of Subsec. III.A, as

$$(E_D{}^{\perp})_{lab} = \frac{1}{\pi}\left(\frac{E_n + Q_{n,d}}{2}\right)I_1(E_n) + \frac{1}{\pi}\left(\frac{E_n}{4x}\right)I_2(E_n)$$

$$= \frac{1}{\pi}\,(\overline{E}_D)_{lab}\,I_1 + I_2\,\frac{E_n}{4x} \quad , \tag{V.14}$$

with

$$(E_D)_{lab}(\mu_{c.m.}) = \left(\frac{E_n + Q_{n,d}}{2}\right) + \frac{E_n}{4x}\,\mu_{c.m.} \quad . \tag{V.15}$$

The curves for I_1 and I_2 are shown in Figs. 21 and 22. The curves of $(E_D{}^{\perp})_{lab}$ vs E_n are shown in Fig. 23 together with $(\bar{E}_D)_{lab}$ and $(\hat{E}_D)_{lab}$ vs E_n for comparison. Hence they may be expressed approximately as:

$$(E_D{}^{\perp})_{lab} \approx 0.42\ E_n - 1.27 \tag{V.16}$$

and

$$(\bar{E}_D)_{lab} \approx 0.500\ E_n - 1.76. \tag{V.17}$$

Data on the nuclear cross sections for this reaction are very meager. However Brown[5], who took into account the known threshold energy and cross-section shape immediately above the threshold energy for endothermic charged-particle reactions, was able to approximate the cross-sectional curve shown in Fig. 24.[5]

B. Unfolding of the $He^3(n,d)D$ Effect

The unfolding of the $He^3(n,d)D$ effect on the recorded spectra, just as in the case for a recoil nucleus considered in Subsec IV.D, is another very important process in which the useful neutron energy range is increased beyond 4.36 MeV for a He^3 gas-filled detector. However the difference between these two effects is that the deuterons cause pulses only at a specific energy, unlike the pulses caused by He^3 nuclei, which give a continuous energy distribution.

To start the analysis, consider a number of counts in the top channel and suppose that these counts now correspond to an energy $E_n > \frac{4}{3} Q_{n,d}$ ($\frac{4}{3}Q_{n,d} = 4.36$ MeV).

If it is assumed that there are no He^3 recoils from above and that there are no deuterons from above, the number of (n,p) events in the counter causing these counts is

$$\frac{C_N}{f_1(E_N)} \quad .$$

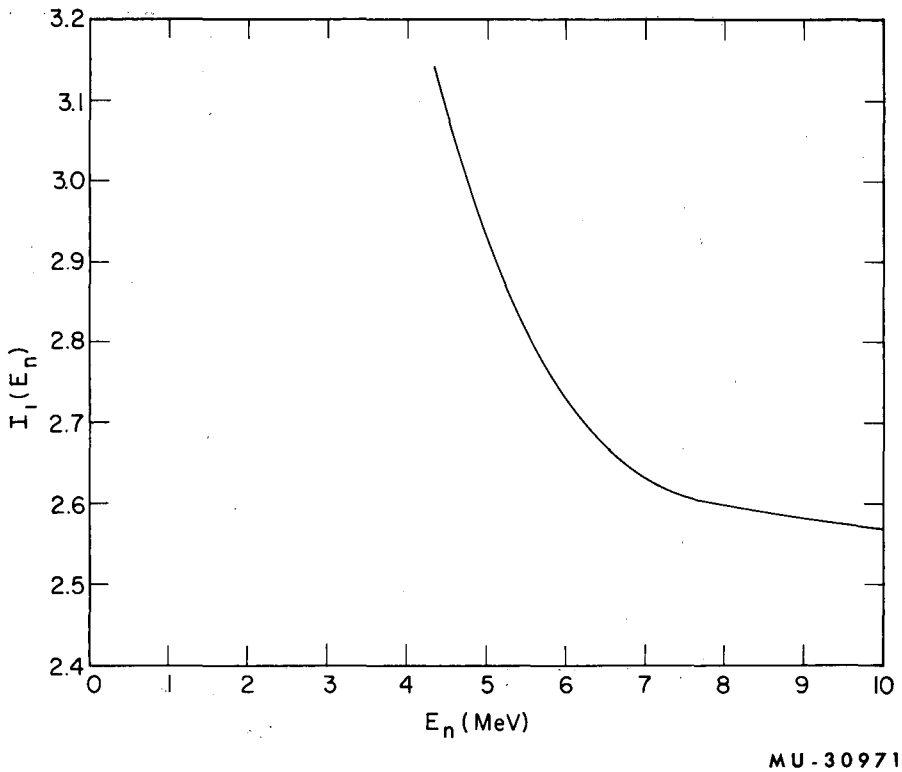

Fig. 21. The energy dependence of $I_1(E_n)$ for deuterons.†

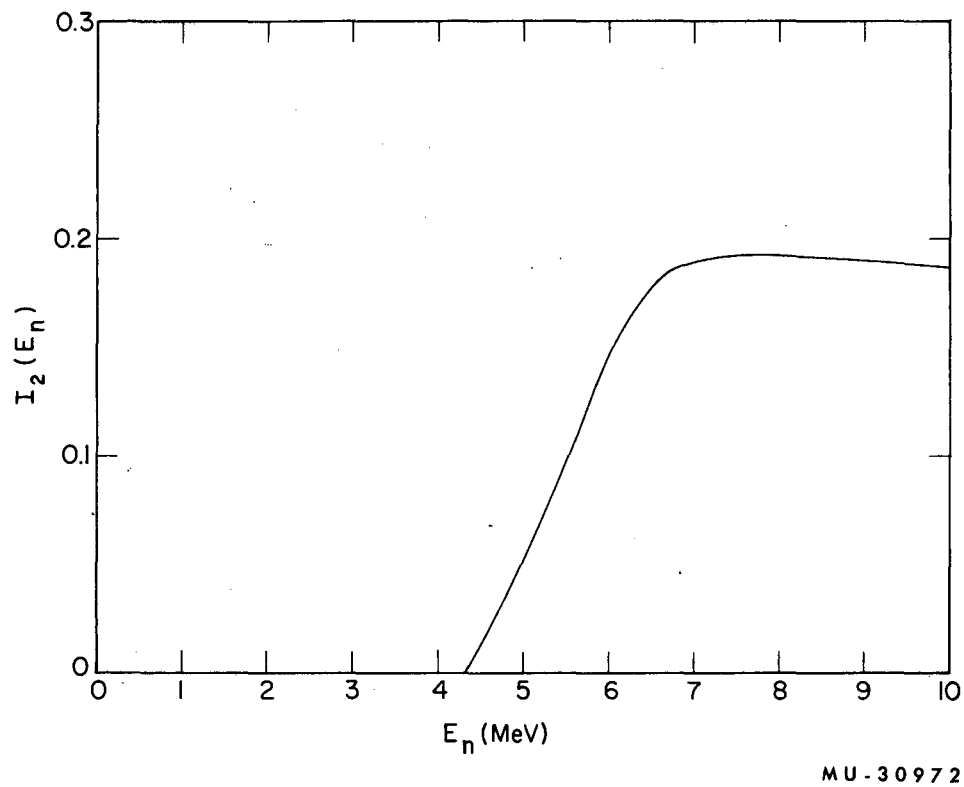

Fig. 22. The energy dependence of $I_2(E_N)$ for deuterons.†

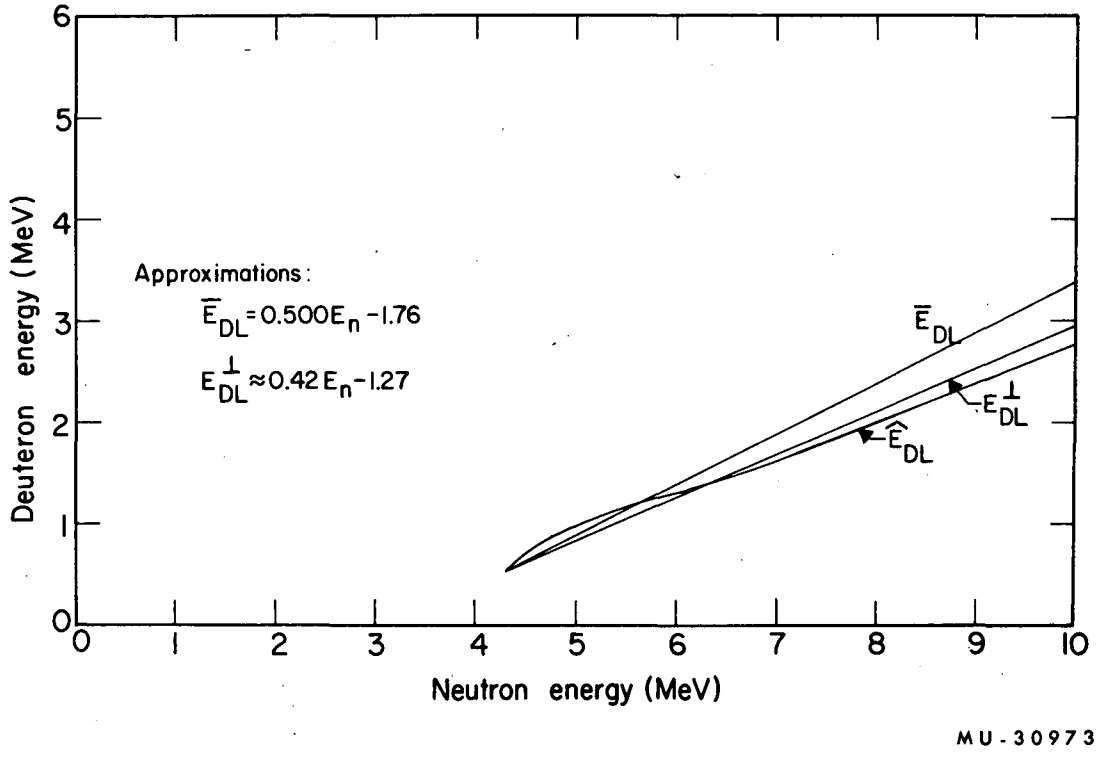

Fig. 23. Relation of deuteron energy to neutron energy.

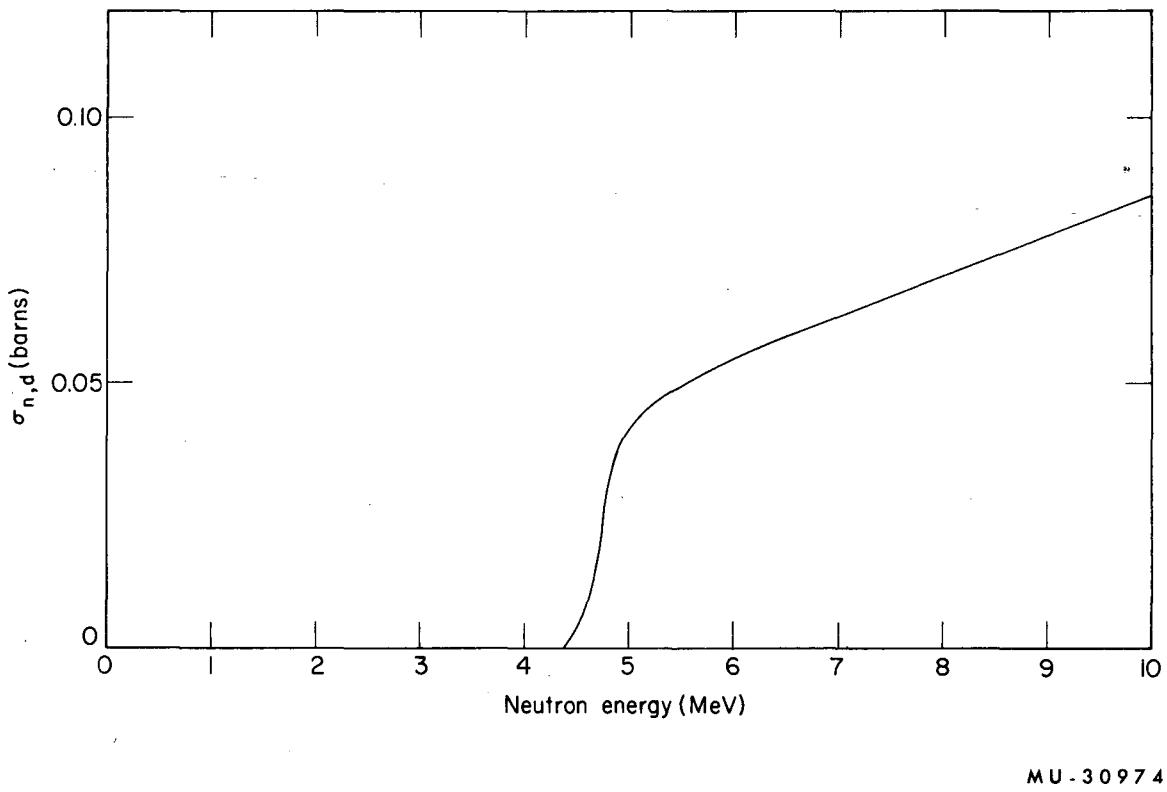

Fig. 24. Helium-3 (n, d) cross section vs neutron energy.†

The number of (n,d) events corresponding to this number of (n,p) events is:

$$\frac{\sigma_{n,d}(E_N) C_N}{\sigma_{n,p}(E_N) f_1(E_N)} .$$

The deuterons cause counts at a lower energy,

$$E_i = E_N + Q_{n,d} .$$

It is seen that the C_N counts recorded will give rise to

$$C_N \frac{\sigma_{n,d}(E_N) f_5(E_N)}{\sigma_{n,p}(E_N) f_1(E_N)}$$

counts in the channel i, corresponding to energy E_i; i.e.,

$$C_{n,d}(E_i) = \frac{C_N \sigma_{n,d}(E_N) f_5(E_N)}{\sigma_{n,p}(E_N) f_1(E_N)} ,$$

where $f_1(E_N)$ is the probability that the protons will not hit the counter wall, as already defined, and where $f_5(E_N)$ is the probability that deuterons deposit all their energy inside the sensitive volume.

Following a similar analysis as that considered in Subsec. III.C, it is found that the form of $f_5(E_N)$ can be expressed as

$$f_5(E_N) = \left[1 - \frac{4}{\pi}\left(\frac{\ell d}{2b}\right)\right]^{[1 + (1 - \bar{\mu}_D^2)^{1/2}]} , \tag{V.18}$$

where

$$\bar{\mu}_D = \frac{x_D}{(1+x_D^2)^{1/2}} \quad \text{and} \quad x_D = \left(\frac{E_n}{3E_n - 12.96}\right)^{1/2} . \tag{V.19}$$

Furthermore, the wall effect will give counts at all energies smaller than the energy of $E_n + Q_{n,d}$. Therefore the following two cases can exist:

(a) Deuterons which deposit all their energy inside the sensitive volume. The number of counts is

$$C_{D1}(j \rightarrow i) = C_j \frac{\sigma_{n,d}(E_j)\, f_5(E_i)}{\sigma_{n,p}(E_j)\, f_1(E_N)} \;, \qquad E_i < E_j < E_N,$$

$$E_j \geq 4.36 \text{ MeV}.$$

(b) Deuterons which deposit only parts of their energies inside the sensitive volume and contribute counts to channel i.

Since this kind of contribution is possible only for deuterons from neutrons of energies which lie between E_N and E_j; i.e., larger than E_j,

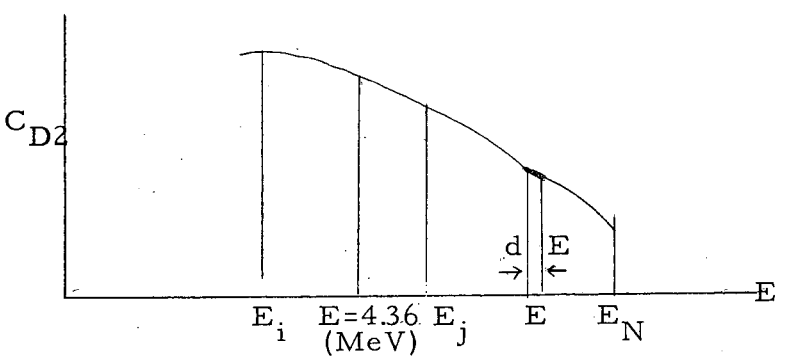

Therefore the number of counts is

$$C_{D2}(i) = \int_{E_j}^{E_N} C(E) \frac{\sigma_{n,d}(E)\, f_6(E)}{\sigma_{n,p}(E)\, f_1(E_N)} P(E \rightarrow E_i)\, dE \;,$$

where

$f_6(E)$ is the probability that a deuteron deposits only part of its energy inside the sensitive volume; i.e., $f_6(E) = 1 - f_5(E)$,

$P(E \rightarrow E_i)$ is the probability per unit energy that the deuteron resulting from a neutron of energy E deposits energy E_i.

Therefore the total number of counts at channel i is

$$C_D(i) = C_{D1}(j \rightarrow i) + C_{D2}(i)$$

$$= \left\{ C_j \frac{\sigma_{n,d}(E_j) f_5(E_i)}{\sigma_{n,p}(E_j) f_1(E_j)} + \int_{E_j}^{E_N} C(E) \frac{\sigma_{n,d}(E) f_6(E)}{\sigma_{n,p}(E_j) f_1(E)} P(E \rightarrow E_i) dE \right\} \tag{V.20}$$

Where the counts fall in the channel i at energy

$$E_i = E_j + Q_{n,d}$$

The unfolding calculation method will be found in Subsec. VI.C.

VI. INVERSION MATRIX

A. Spectrometer Efficiency

The spectrometer efficiency is, in general, dependent on the following independent factors:

(a) Nuclear cross sections,

(b) Counter dimensions,

(c) Gas pressures.

Therefore, the overall spectrometer efficiency of this detector as a function of neutron energy may be written

$$\eta = N_{He^3}\,\sigma_{He^3}(E)\,D\,f_1(E), \tag{VI.1}$$

where

η = overall spectrometer efficiency,

N_{He^3} = number of He^3 atoms per cubic centimeter of sensitive volume at filling pressure,

$\sigma_{He^3}(E)$ = $He^3(n,p)T$ cross section, which has been plotted in Fig. 25,

D = effective thickness of the detector for 4π geometry

$$= \frac{\text{total sensitive volume}}{\text{effective area}}$$

$$= \frac{\pi b^2 L}{\pi\left(\frac{3}{4}\right)^{2/3} L^{2/3} b^{4/3}} = \left(\frac{4}{3}\right)^{2/3} b^{2/3} L^{1/3},$$

where

b = radius of counter,

L = effective length of the counter,

$f_1(E)$ = probability that protons will not suffer wall effects.

The variations of $f_1(E)$ vs pressure and counter dimensions are presented in Figs. 26, 27, 28, and 29.

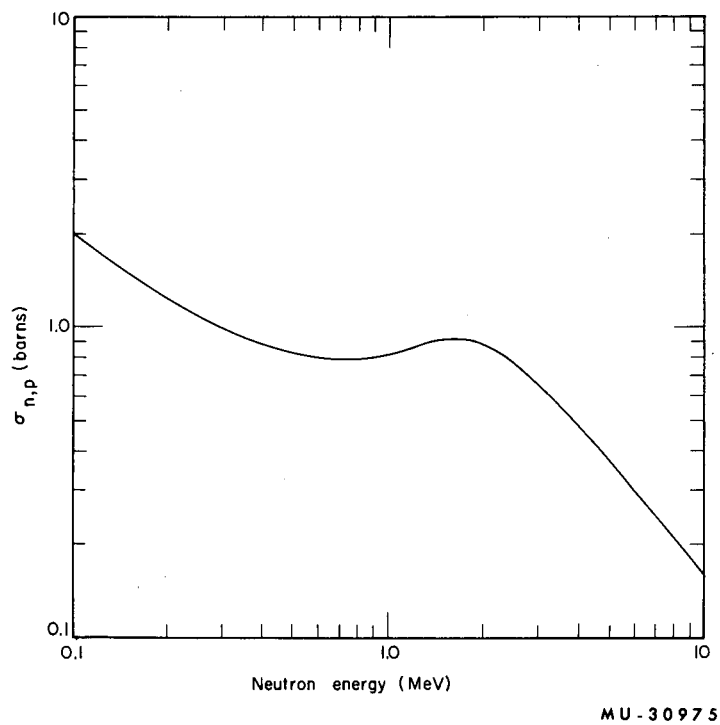

Fig. 25. Helium-3 (n, p) cross section vs neutron energy.†

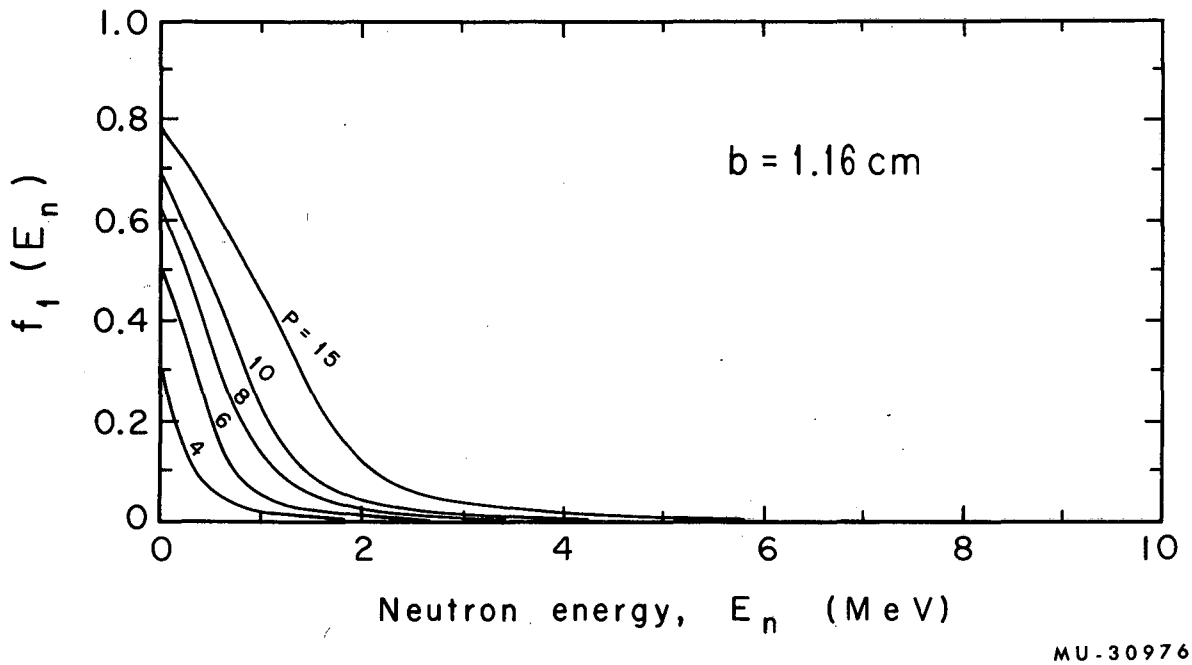

Fig. 26. The function $f_1(E_n)$, the probability that protons will not hit the counter wall, for counter radius b = 1.16 cm.

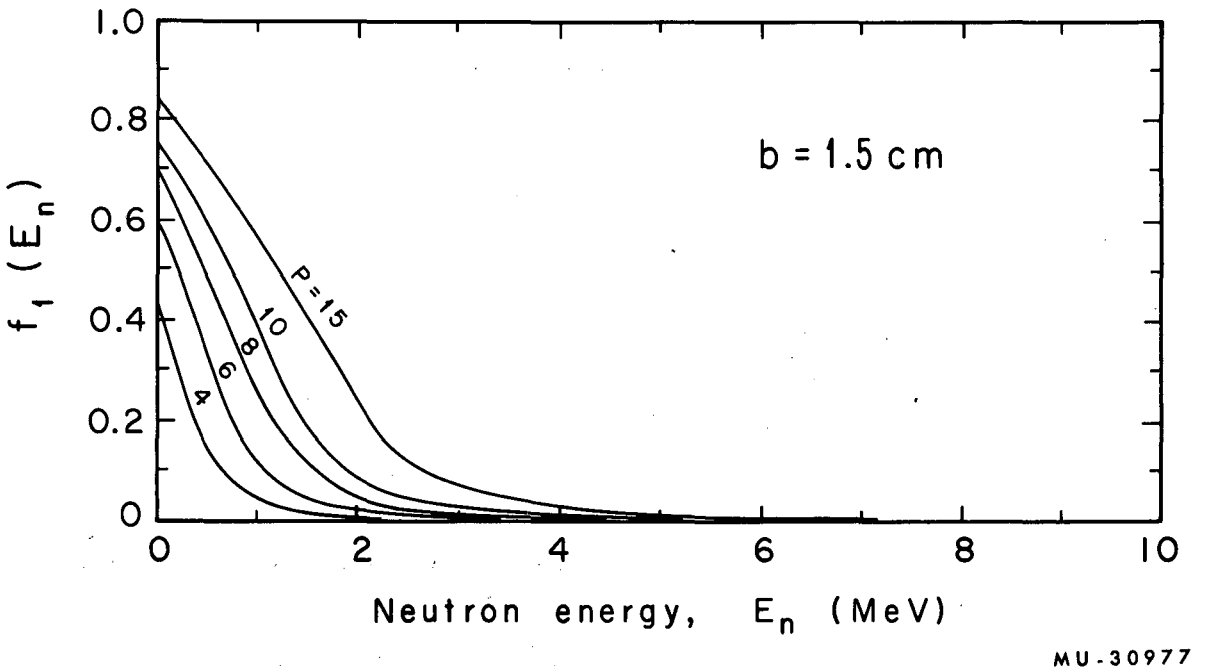

Fig. 27. The function $f_1(E_n)$, the probability that protons will not hit the counter wall, for counter radius b = 1.5 cm.

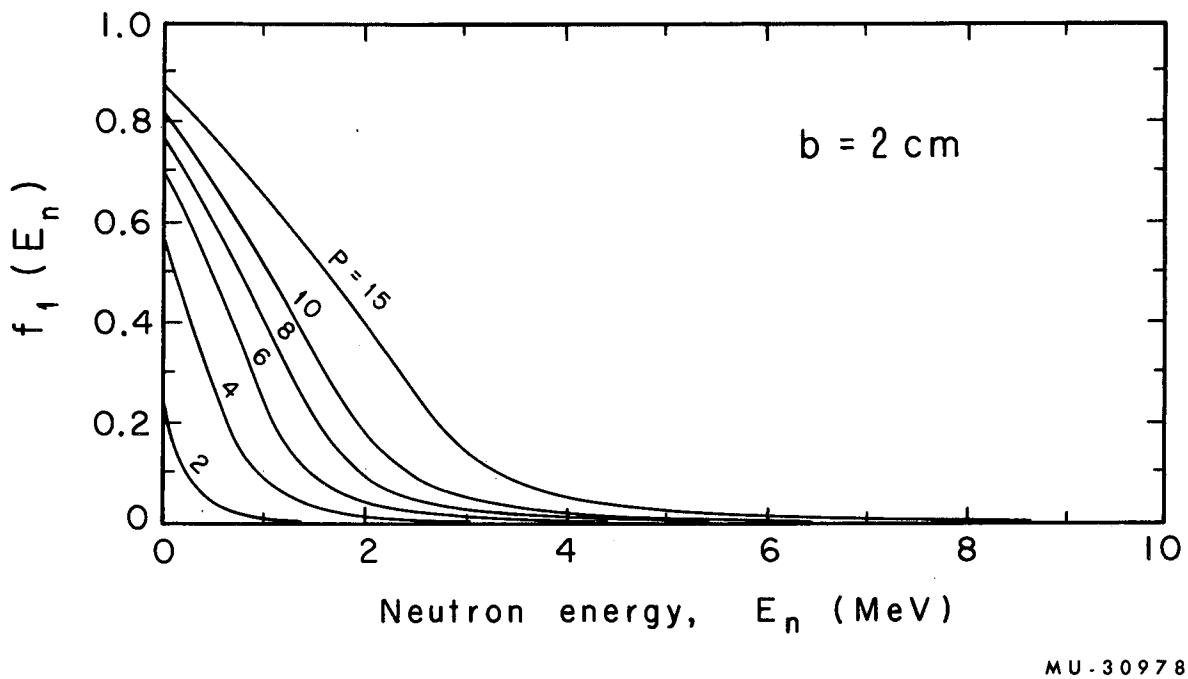

Fig. 28. The function $f_1(E_n)$, the probability that protons will not hit the counter wall, for counter radius b = 2 cm.

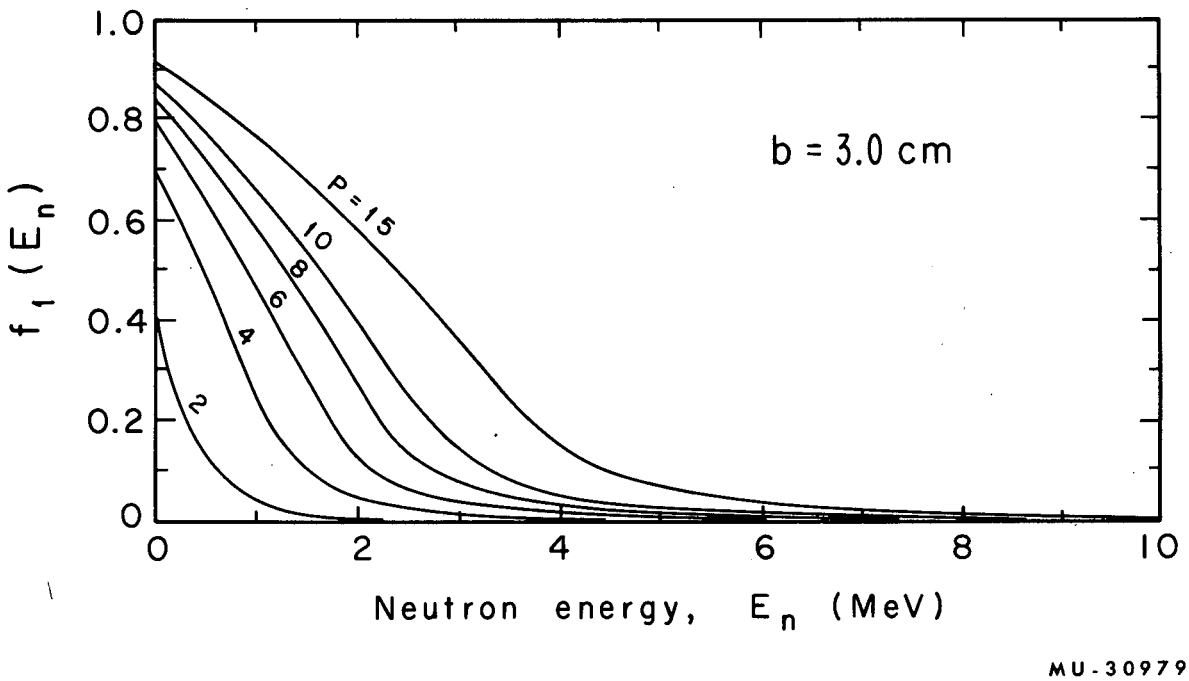

Fig. 29. The function $f_1(E_n)$, the probability that protons will not hit the counter wall, for counter radius b = 3.0 cm.

B. Recombination Considerations†

The phenomena of recombination of ions should be taken into account. Helium-3 ions produce tracks having considerably greater specific ionizations than those of protons. Since the specific ionization is proportional to Z^2, it will give rise to different columnar (or preferential) recombination for these two ions. To a first approximation, this has the effect of collapsing to a slight extent the energy scale for the He^3 ions relative to the scale of protons. The effect can be taken into account by subtracting off the recoil spectrum at an energy given by the recombination constant (K) times the calibration scale. Because the He^3 energy scale has been collapsed, the ordinate must be increased by the same factor (1/K).

The recombination constant is a function of filling gas pressure, operating voltage, and filling gas composition. The probability for an electron to combine with a positive ion in a given time interval is proportional to the density of positive ions. Because of the lack of experimental data on this recombination constant, the usual way of estimating it is by comparing the location of the mean upper energy limit of the recoil spectrum with the location of the peak of the calibration spectrum due to the monoenergetic neutrons.

C. The Matrix

According to all the foregoing analysis, it is possible to express the resultant pulse-height spectrum of protons from the raw spectrum (without unfolding any effect) by means of a so-called inversion matrix, by the following procedures.

(1) Starting from the top channel of a recorded raw spectrum C_N, the unfolding of the deuteron effects is from the formula

$$C_D(j \rightarrow i) = \left\{ C_j \frac{\sigma_{n,d}(E_j) f_5(E_i)}{\sigma_{n,p}(E_j) f_1(E_j)} + \int_{E_j}^{E_N} C(E) \frac{\sigma_{n,d}(E) f_6(E)}{\sigma_{n,p}(E_j) f_1(E)} P(E \rightarrow E_i) dE \right\} \tag{V.20}$$

The unfolding calculation, starting from the fixed top channel $j = N$, carries out this computation for each channel i. This result is subtracted from the raw spectrum for each i, from $i = N-1$ to $i = 0$. This difference serves as the new or unfolded spectrum for the next calculation. The next calculation is made by changing j from $j = N$ to $j = N-1$, and computing this C_D for each i from $i = N-2$ to $i = 0$. These processes are repeated until $E_j = 4.36$ MeV, the threshold energy of the (n, d) reaction. This step finishes the unfolding of deuteron effect.

(2) Starting also from the top channel of the same recorded raw spectrum C_N, the unfolding of the recoil effect is from the formula

$$C_{He}(j \rightarrow i) = \left\{ \frac{C_j \sigma_S(E_j)}{\sigma_{n,p}(E_j) f_1(E_j)} \left[f_2(E_j) p(E_i) + f_3(E_j) \int_{E_i}^{\frac{3}{4}E_j} p(E) P(E \rightarrow E_i) dE \right] \right\} \Delta_i E.$$

This $C_{He}(j \rightarrow i)$ should be first calculated for each i running from $i = 3/4(N)$ down to $i = 0$ for a fixed upper limit $j = N$. The results are then subtracted from the data (or counts) of the corresponding raw spectrum. This difference serves as a new spectrum for the next calculation. The next calculation is made by changing E_j from $j = N$ to $j = N-1$, and letting i run from $i = 3/4(N-1)$ to $i = 0$. These procedures are repeated until the upper limit of the calculation reaches the channel equivalent to that of 1-MeV neutrons. This step finishes the unfolding of the helium-nucleus recoil effect.

(3) Starting from the top channel of the unfolded (1) and (2) spectrum C_N the unfolding of the wall effects of protons and tritons is from the formula

$$C_p(j \rightarrow i) = \int_{E_i}^{E_N} \frac{C_j(E)\,[1 - f_1(E)]}{f_1(E)} P(E \rightarrow E_i)\, dE.$$

This $C_p(j \rightarrow i)$ should be calculated for each i running from $i = N-1$ to $i = 0$ for a fixed top channel $j = N$, as upper limit. This calculated result is then subtracted from the C_N spectrum at the corresponding channel, and the difference serves as a new spectrum

for the next calculation. The next calculation is made by changing E_N from $E_N = E_N$ to $E_N = E_{N-1}$, and computing $C_p(j \rightarrow i)$ for each i from $i = N-2$ to $i = 0$. These procedures are repeated until the upper limit of the integration reaches the lower limit of the original spectrum. This step finishes the unfolding of the wall effects of protons and tritons. Therefore, after unfolding the effects, a resultant proton-pulse-height spectrum is obtained from the raw spectrum. To express this idea symbolically, let

$C_0(i)$ = resultant proton pulse-height at channel i,

$C_i(i)$ = raw spectrum at channel i,

then

$$C_0(i) = C_i(i) - [C_D(j \rightarrow i) + C_{He}(j \rightarrow i) + C_p(j \rightarrow i)],$$

for $i = 0, 1, 2, \cdots N$, the channel number; or, to express this idea in matrix form,

$$\overline{C}_0 = A\,\overline{C}_i,$$

where

$$\overline{C}_0 = \begin{bmatrix} C_0(N) \\ C_0(N-1) \\ \cdot \\ \cdot \\ \cdot \\ C_0(0) \end{bmatrix}, \quad \overline{C}_i = \begin{bmatrix} C_i(N) \\ C_i(N-1) \\ \cdot \\ \cdot \\ \cdot \\ C_i(0) \end{bmatrix},$$

and A is the so-called inversion matrix whose elements should include the unfolding and subtracting operators.

D. The Corrected Spectrum

Since the efficiency of the detector is, from Subsec. VI.A,

$$\eta = N_{He^3}\,\sigma_{He^3}(E)\,f_1(E)\,D,$$

let $C_I(E)$ be the corrected spectrum in question. Then, since

$$C_I(E)\,\eta(E) = C_0(E),$$

therefore

$$C_I(E) = \frac{C_0(E)}{\eta(E)} \quad ,$$

where $C_0(E)$ is the resultant proton spectrum. The expressions for $f_1(E)$, $f_2(E)$, $f_3(E)$, $f_5(E)$, $P(E)$, and $P(E \rightarrow E_i)$ from the foregoing analysis are listed as follows.

$$f_1(E) = f_1^{p,T} = f_1^{p} \times f_1^{T} (1 - \bar{\mu}_T^{\,2})^{1/2} \quad . \qquad \text{(VI.2)}$$

There are two cases for f_1^{P}.

Case 1. For $E_n \leq E_{crit}$*, based on a single track:

$$f_1^{P} = 1 - \frac{2}{\pi} \left[\left(\frac{\ell_p}{2b}\right) \left[1 - \left(\frac{\ell_p}{2b}\right)^2 \right]^{1/2} + \sin^{-1}\left(\frac{\ell_p}{2b}\right) \right] , \qquad \text{(VI.3)}$$

where ℓ_p is determined from the range formulas for protons at any energy

$$E_p = 0.505\, E_n + 0.450 \text{ (MeV)} \qquad \text{(VI.4)}$$

Case 2. For $E_n \geq E_{crit}$, based on intersection surfaces of a cylinder and a sphere:

$$f_1^{P} = (1 - x_p^{\,2})^{1/2} \left\{ 1 - \left[1 - \left(\frac{b}{\ell_p}\right)^2 \right]^{1/2} \right\} \left(1 + 0.392 \frac{b}{\ell_p} \right) , \qquad \text{(VI.5)}$$

with

$$x_p = \frac{1}{(3)^{1/2}} \left(\frac{E_n}{3E_n + 4Q_{n,p}} \right)^{1/2} , \quad Q_{n,p} = 0.764. \qquad \text{(VI.6)}$$

Where ℓ_p is determined from the range formulas for protons at an energy

$$E_p = 0.586\, E_n + 0.574 \quad \text{(MeV)}, \qquad \text{(VI.7)}$$

$$f_1^{T} = 1 - \frac{4}{\pi} \left(\frac{\ell_T}{2b} \right) . \qquad \text{(VI.8)}$$

Where ℓ_T is determined from the range formulas for tritons at an energy

$$E_T = 0.340\, E_n + 0.150 \quad \text{(MeV)} \qquad \text{(VI.9)}$$

---

* E_{crit} is defined as the neutron energy where the functions in above two cases continue; the value of E_{crit} in MeV depends on the gas pressure of the detector (see Appendix A for a more detailed definition).

$$\bar{\mu}_T = \frac{x_T}{(1+x_T^2)^{1/2}} \quad \text{and} \quad x_T = 3x_p = (3)^{1/2}\left(\frac{E_n}{3E_n+4Q_{n,p}}\right)^{1/2}, \tag{VI.10}$$

$$f_2(E) = 1 - \frac{4}{\pi}\left(\frac{\ell_{He}}{2b}\right). \tag{VI. 11}$$

Where ℓ_{He} is determined from the range formulas for He^3 ions at an energy

$$E_{He} = \frac{3E_n}{8\pi}\left(\frac{8}{3} - I_2\right), \tag{VI. 12}$$

where

$$I_2 = \int_{-1}^{1} \left[(\mu_{c.m.})\mu_{c.m.} d\mu_{c.m.}\right] \left[(\mu_{c.m.}) = \int_0^{\frac{\pi}{2}} (1-K^2 \sin^2\theta)^{1/2} d\theta, \right. \tag{VI.13}$$

$$K = \left(1 - \frac{4}{3}\frac{E_r}{E_n}\right)^{1/2} = \left[1 - \frac{1}{2}(i - \mu_{c.m.})\right]^{1/2}, \tag{VI.14}$$

$$f_3(E) = 1 - f_2(E) = 1 - \left[1 - \frac{4}{\pi}\left(\frac{\ell_{He}}{2b}\right)\right] = \frac{4}{\pi}\left(\frac{\ell_{He}}{2b}\right) \text{ ; from above,} \tag{VI. 15}$$

$$f_5(E) = \left[1 - \frac{4}{\pi}\left(\frac{\ell_D}{2b}\right)\right]^{[1+(1-\bar{\mu}_D^2)^{1/2}]} . \tag{VI.16}$$

Where ℓ_D is determined from the range formulas for deuterons at an energy

$$E_D = 0.42\, E_n - 1.27, \tag{VI.17}$$

$$E_n \geqslant 4.32 \text{ (MeV)}, \tag{VI.18}$$

$$\bar{\mu}_D = \frac{x_D}{(1+x_D^2)^{1/2}}, \quad x_D = \left(\frac{E_n}{3E_n+4Q_{n,d}}\right)^{1/2}, \quad Q_{n,d} = -3.24 \text{ (MeV)}, \tag{VI. 19}$$

$$f_6(E) = 1 - f_5(E) = 1 - \left[1 - \frac{4}{\pi}\left(\frac{\ell_D}{2b}\right)\right]^{[1+(1-\bar{\mu}_D^2)^{1/2}]}, \tag{VI.20}$$

$$p(E) = \frac{16\pi}{3E_j} \frac{1}{\sigma_S(E_j)} \sum_{\ell=0}^{3} a_\ell(E_0) P_\ell \left(1 - \frac{8E}{3E_j}\right) , \qquad \text{(VI.21)}$$

$$P(E \rightarrow E_i) = \left[\frac{1}{E_b^2 E_i^2} (E_b E^2 - \frac{2}{3} E^3) + \frac{E^2}{2E_L E_i^2} + \frac{1}{2E_L}\right], \qquad \text{(VI.22)}$$

where E_b, E_L are from the energy-range formulas for ranges b and L, respectively, for each different particle in question.

The variation of $f_2(E)$ and $f_5(E)$ vs neutron energies and filling pressures are plotted in Figs. 30 and 31, respectively.

In order to increase the counting efficiency of the detector, krypton gas is usually added to the He^3 gas. The krypton is to increase the stopping power of the filling gas, and the He^3 serves as the reaction gas. The ranges of charged particles in the mixture of these gases can be estimated as follows.

Range formulas for individual gases† (mg/cm^2):

Protons

$$R_p(E) \text{ in Kr} = R_{p'}(E) \text{ in air } [1.89 - 0.25 \log(E)] - 0.36,$$

$$R_{p'}(E) \text{ in He} = R_{p'}(E) \text{ in air } [0.82 - 0.25 \log(E)].$$

He^3 Ions

$$R_{He^3}(E) \text{ in Kr} = \frac{3}{4} \left\{R_p \text{ in air}\left(\frac{E}{3}\right) [1.89 - 0.25 \log\left(\frac{E}{3}\right)] - 0.36\right\},$$

$$R_{He^3}(E) \text{ in He} = \frac{3}{4} \left\{R_p \text{ in air } \left(\frac{E}{3}\right)[0.82 - 0.25 \log\left(\frac{E}{3}\right)]\right\}.$$

Tritons

$$R_T(E) \text{ in Kr} = 3 \left\{R_p \text{ in air } \left(\frac{E}{3}\right) [1.89 - 0.25 \log \left(\frac{E}{3}\right)] - 0.36\right\},$$

$$R_T(E) \text{ in He} = 3 R_{p'} \left(\frac{E}{3}\right) \text{ in air } [0.82 - 0.25 \log \left(\frac{E}{3}\right)].$$

Deuterons

$$R_d(E) \text{ in Kr} = 2 \left\{R_{p'} \left(\frac{E}{2}\right) \text{ in air } [1.89 - 0.25 \log\left(\frac{E}{2}\right)] - 0.36\right\},$$

$$R_d(E) \text{ in He} = 2 R_{p'} \left(\frac{E}{2}\right) \text{ in air } [0.82 - 0.25 \log \left(\frac{E}{2}\right)].$$

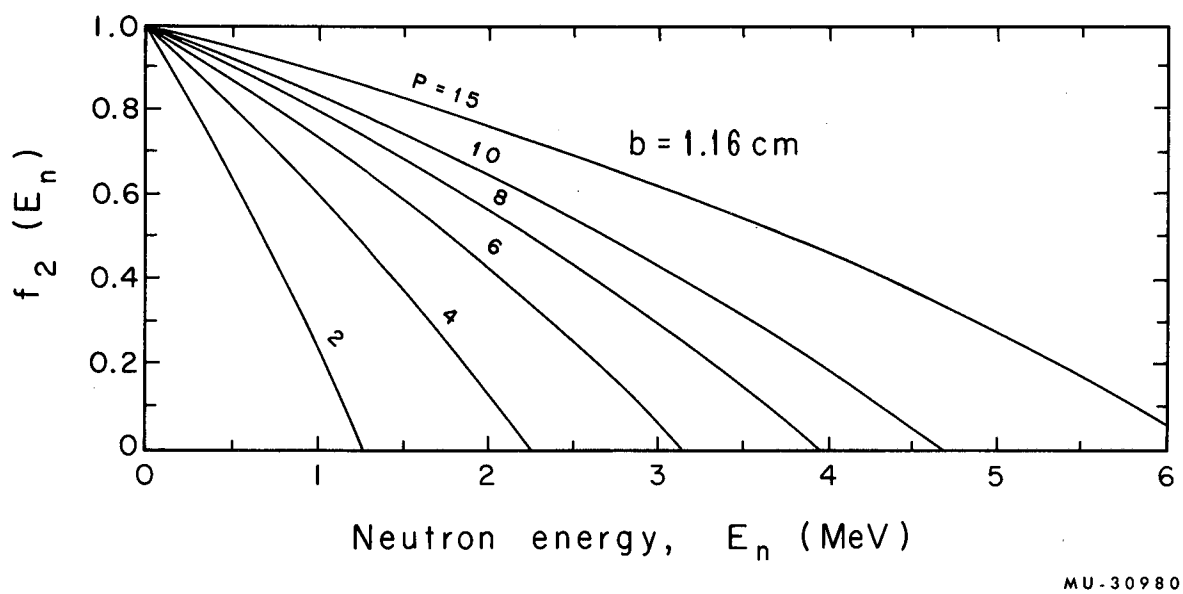

Fig. 30. The function $f_2(E_n)$, the probability that He^3 nuclei will not hit the counter wall, vs neutron energy E_n.

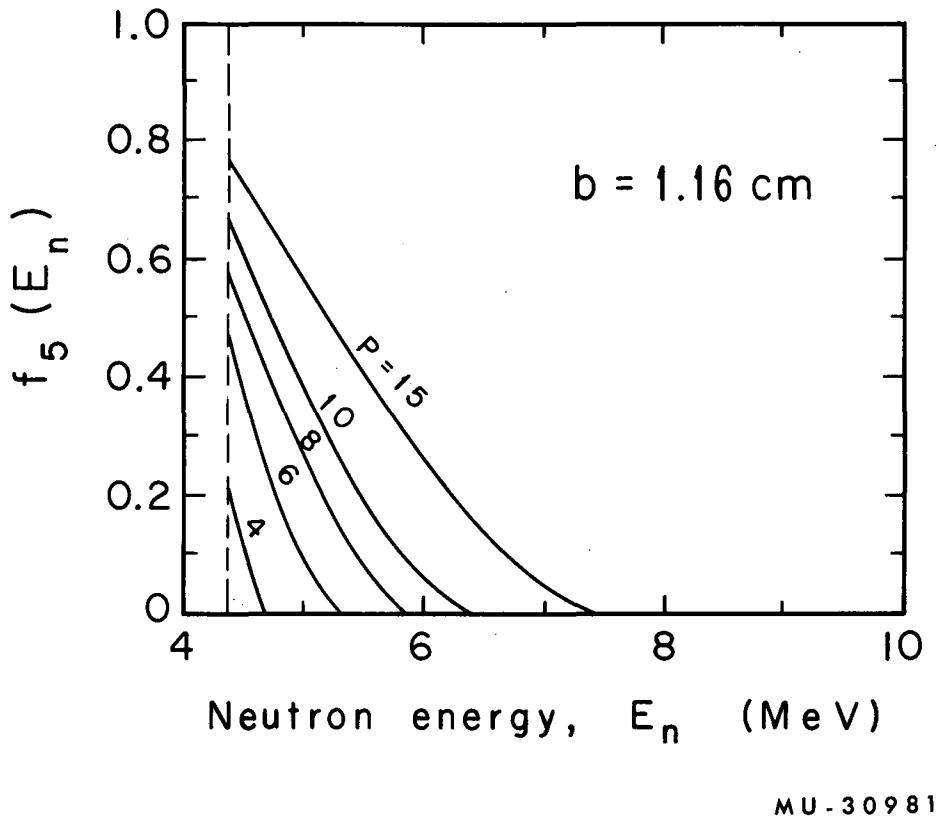

Fig. 31. The function $f_5(E_n)$ the probability that deuterons will not hit the counter wall, vs neutron energy E_n.

Conversion of particle ranges from mg/cm^2 to cm is as follows:

$$\ell(cm) = \frac{R_{tot}\,(mg/cm^2)}{\left(\frac{p_{He}}{14.7}\right)\rho_{He} + \left(\frac{p_{Kr}}{14.7}\right)\rho_{Kr}} ,$$

where

R_{tot} = total particle range in the gas mixture in mg/cm^2,

p = partial pressure of individual gas as given in the input data (psia),

ρ = gas density at STP.

<u>Ranges in Gas Mixture</u>†

$$\frac{1}{R_{tot}(E)} = \frac{W_{He}}{R \text{ in He}(E)} + \frac{W_{Kr}}{R \text{ in Kr}(E)} ,$$

where W = Weight fraction, $W_{He} + W_{Kr} = 1$,

$$W_{He} = \frac{p_{He}\,\rho_{He}}{p_{He}\,\rho_{He} + p_{Kr}\rho_{Kr}} ,$$

$$W_{Kr} = \frac{p_{Kr}\,\rho_{Kr}}{p_{He}\,\rho_{He} + p_{Kr}\,\rho_{Kr}} = 1 - W_{He},$$

where

p = partial pressure of the gas as given in the input data (psia),

ρ = gas density at STP,

ρ_{He} = 0.116629 g/liter,

ρ_{Kr} = 3.455 g/liter.

VII. SAMPLE CALCULATION

A. The Detector

For the purpose of illustrating the method mentioned in the previous sections, a machine-computed calculation that computes the response matrix and inverts the spectrum of a TNC (Texas Nuclear Corporation) detector model 312 follows. The TNC detector construction details are:

Detector material	Copper
Length	7-1/8 in.
Diameter	1 in.
Active length	3-1/2 in.
Active diameter	15/16 in.
Filling pressure	10 atm.

The filling gas He^3 which contains 10^{-9}% of tritium. Therefore the purity of the filling gas is high, and the effect of the tritium can then be neglected.

B. The Raw Spectrum

A raw spectrum is obtained by putting this detector inside of concentric sheaths made of 0.04-in.-thick cadmium and 0.023-in. -thick indium, and then irradiating with plutonium fluoride neutrons. This raw spectrum is plotted in Fig. 32.*

The calibration of the spectrum fixes the top channel (100) of the spectrum as neutron energy of 2.28 MeV.** There are essentially no counts above this energy. Therefore we need only consider the wall effects due to protons and tritons, and the recoil effects due to He^3 nuclei.

---

* The data and calibration of this figure were supplied by Mr. A. H. Redmond of the U. S. Naval Radiological Defense Laboratory, San Francisco.

** Refer to Appendix B for neutron energy calibration.

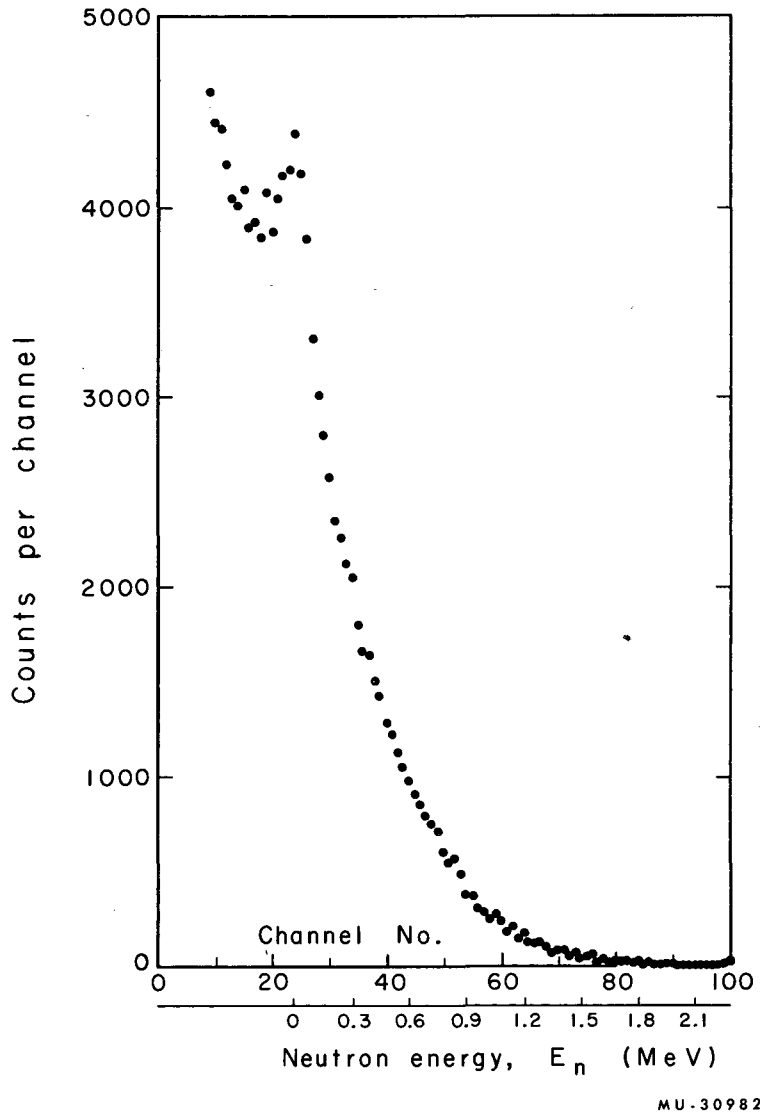

Fig. 32. The raw spectrum from the TNC detector. (See Appendix B-1 for E_n scale; data supplied by A. H. Redmond.)

C. Unfolding Procedures

The recoil effects should be unfolded first according to the formula

$$C_{He}(j\rightarrow i)=\left\{\frac{C_j}{\sigma_{n,p}(E_j)}\left[\frac{f_2(E_j)p(E_i)}{f_1(E_j)}+f_3(E_j)\int_{E_i}^{\frac{3}{4}(E_j)}\frac{p(E)P(E\rightarrow E_i)}{f_1(E_j)}\,dE\right]\right\}\Delta_i E.$$

After unfolding this effect, the spectrum is as shown in Fig. 33. Afterward, the wall effect of protons and tritons is unfolded by the formula

$$C_p(j\rightarrow i) = \int_{E_i}^{E_N=2.28\ \mathrm{MeV}} \frac{C(E)[1-f_1(E)]}{f_1(E)}\,P(E\rightarrow E_i)\,dE\ .$$

After the unfolding of the wall effects of protons and tritons, and the removal of the thermal-neutron peak spectrum, the spectra are shown in Fig. 34. The thermal peak is taken from the experimental response of this detector incorporated into a moderated PuBe neutron source.

Fig. 35 expresses the comparison of spectra from various steps of unfolding results.

Fig. 36 shows the resultant spectrum together with He^3 recoil and wall effect of protons and tritons.

Fig. 37 shows the corrected spectrum that is obtained from the resultant spectrum (in Fig. 36) divided by η, the counter efficiency.

The $f_1(E_n)$'s are from the following two cases.

<u>Case 1.</u> $E_n \leq 1.27$ (MeV),*

$$f_1(E_n) = \left(1-\frac{2}{\pi}\left\{\frac{\ell_P}{2b}\left[1-\left(\frac{\ell_P}{2b}\right)^2\right]^{1/2}+\sin^{-1}\left(\frac{\ell_P}{2b}\right)\right\}\right)\left[1-\frac{4}{\pi}\left(\frac{\ell_T}{2b}\right)\right]^{(1-\bar{\mu}_T^{\,2})^{1/2}},$$

* This value of E_n has been calculated for the continuity of $f_1(E_n)$'s for case 1 and case 2, which will be seen shortly.

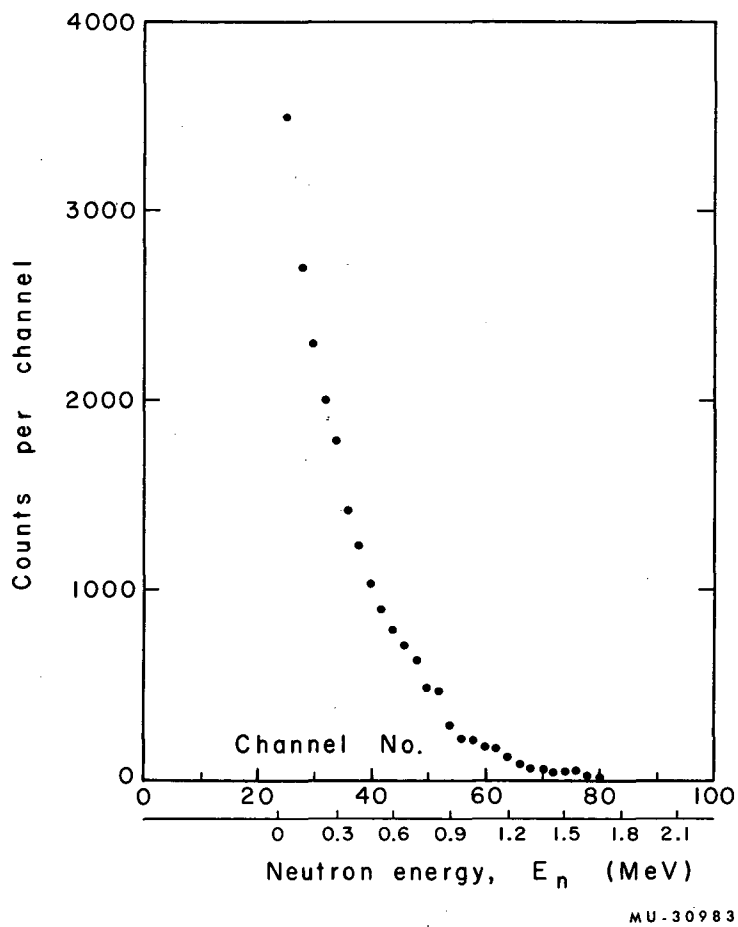

Fig. 33. The spectrum after unfolding He^3 recoils.

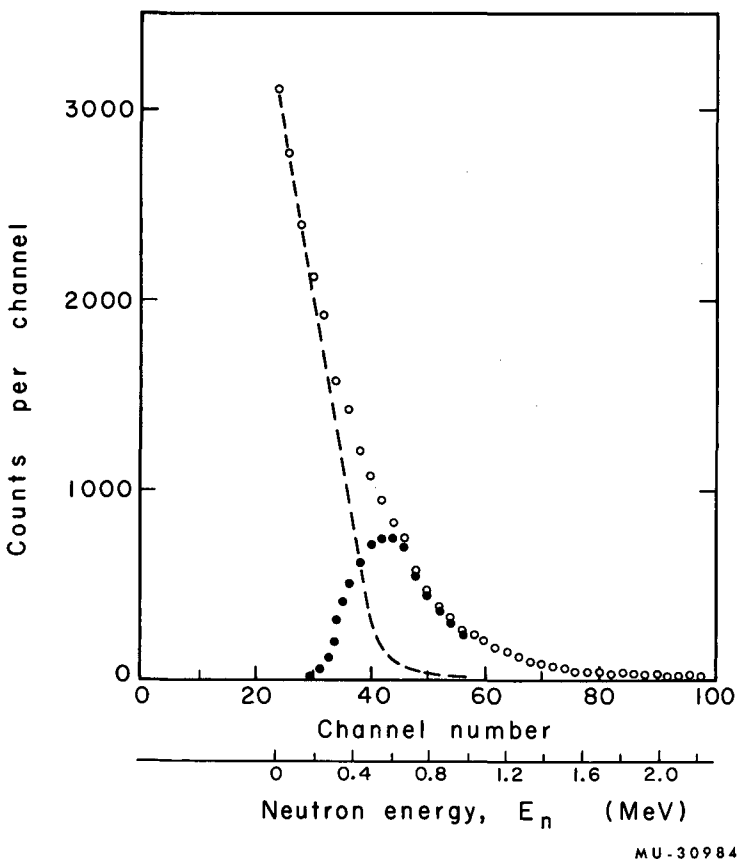

Fig. 34. The spectra after unfolding the wall effect of protons and tritons (from PuF_4-3 source).

o Spectrum after unfolding the wall effect of protons and tritons only.

--- Thermal-neutron peak spectrum from moderated PuBe source.

● Spectrum after unfolding the wall effect of protons and tritons as well as thermal peak.

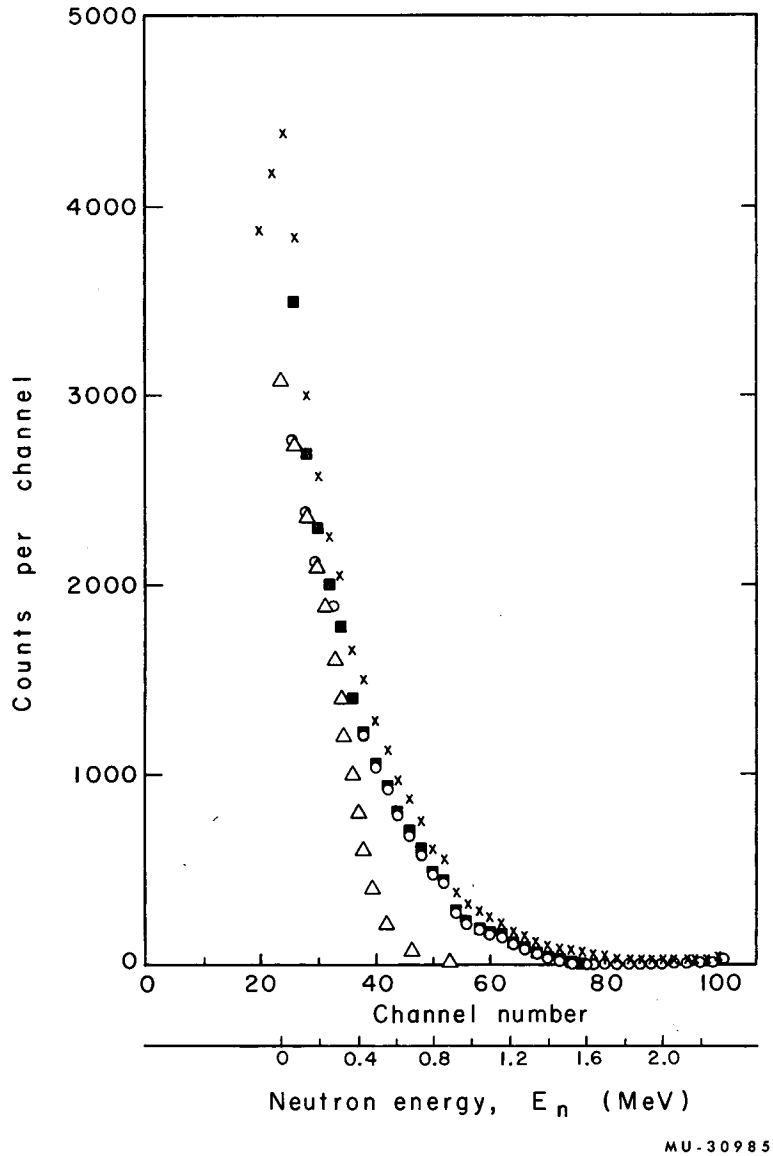

Fig. 35. Comparison of spectra from various steps of unfolding results (from PuF_4-3 source).
x Original raw spectrum.
■ After unfolding He^3 recoils.
o After unfolding wall effects of protons and tritons.
△ Thermal peak spectrum.

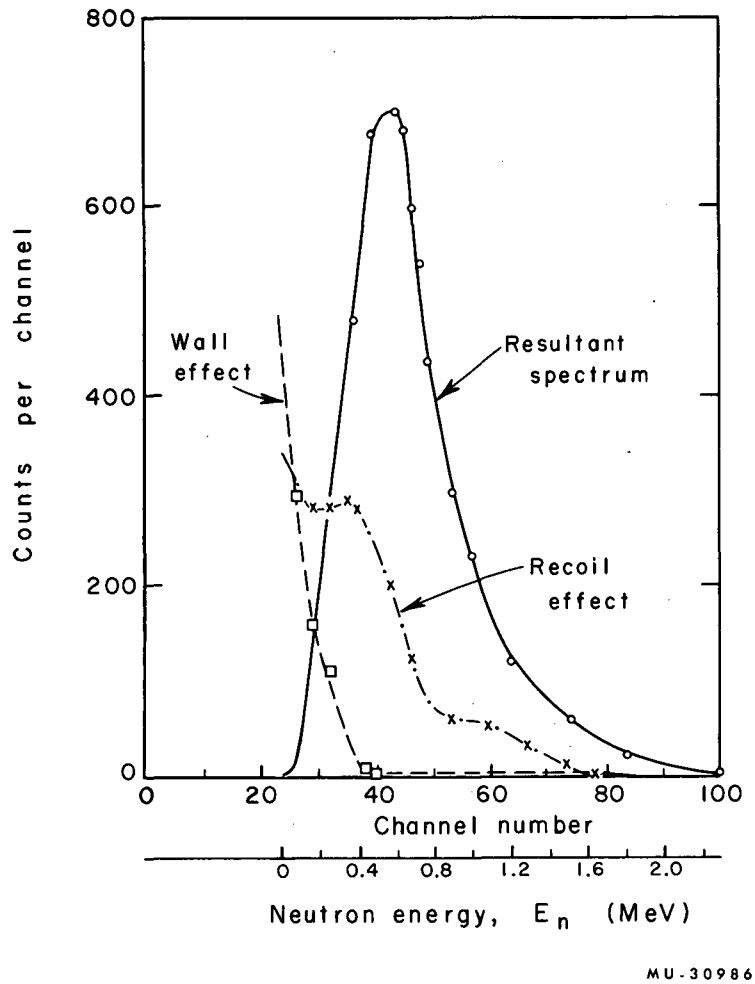

Fig. 36. Resultant spectrum together with He^3 recoil effect and wall effect of protons and tritons (with PuF_4-3 source).

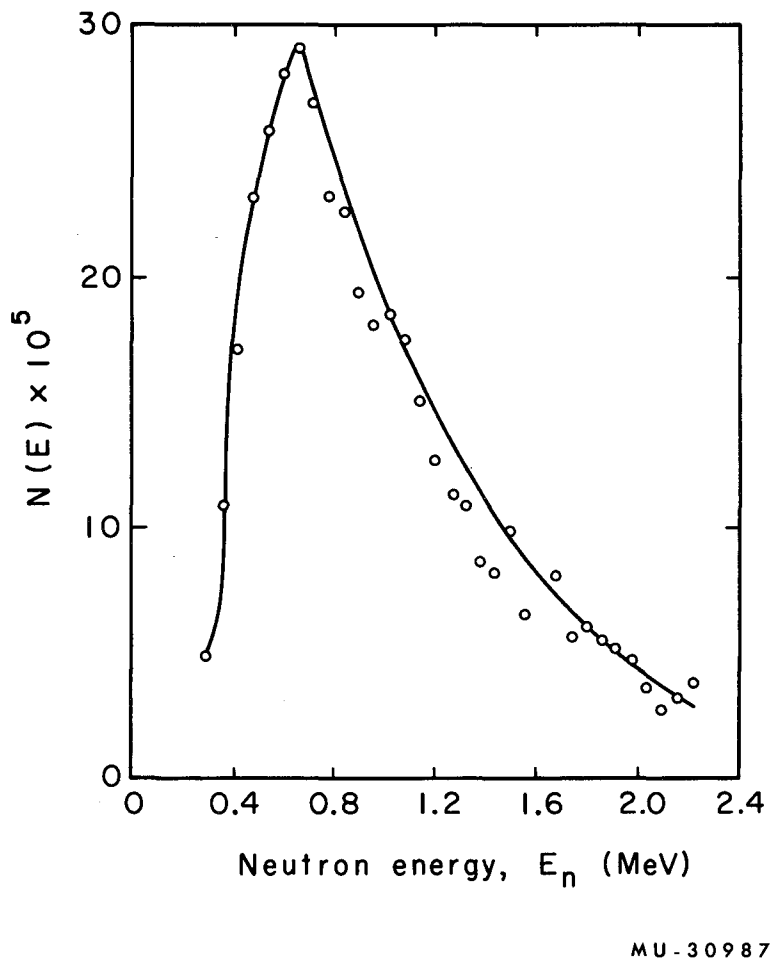

Fig. 37. Corrected spectrum from PuF_4-3 source.

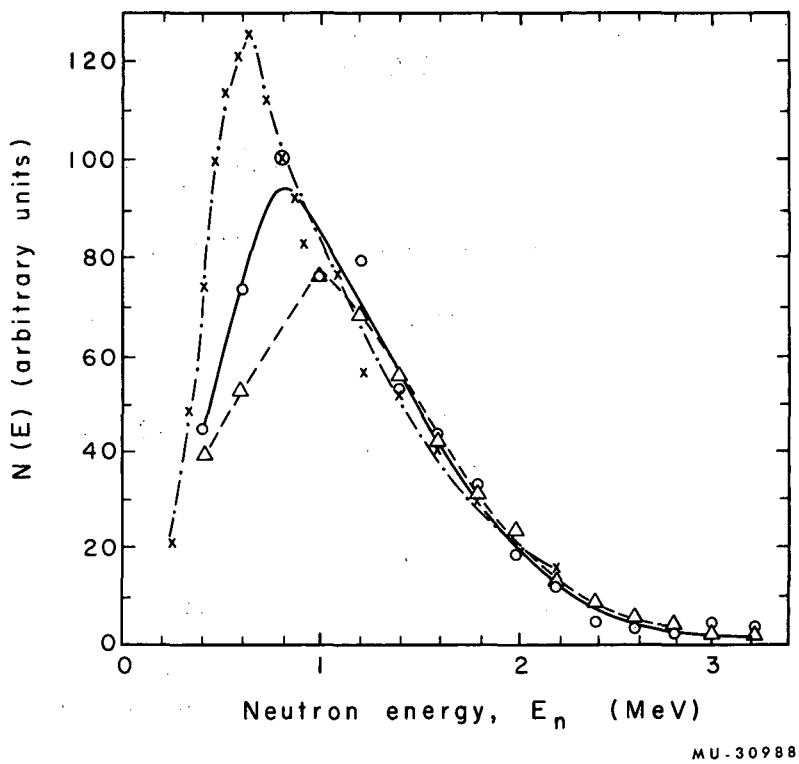

Fig. 38. Comparison of results.

Δ-- PuF_4-2, Hanford source spectrum, from emulsion technique.

o— PuF_4-3, Source spectrum, from emulsion technique.

x—·—PuF_4-3, Source spectrum, from TNC He^3 detector.

where

$b = 1.16$ cm,

$$\bar{\mu}_T = \frac{x_T}{[1+x_T^2]^{1/2}} \quad , \quad x_T = (3)^{1/2}\left(\frac{E_n}{3E_n+3.056}\right)^{1/2} ,$$

ℓ_p is from $\ell_p = \frac{1.07}{10}(7\,E_p + 6.7\,E_p^2)^*$,

E_p is from $E_p = 0.505\,E_n + 0.450$, (MeV)

ℓ_T is from $\ell_T = \frac{1.07}{10}(7E_T + \frac{6.7}{3}E_T^2)^*$,

E_T is from $E_T = 0.340\,E_n + 0.15$ (MeV).

<u>Case 2.</u> $10 \geqslant E_n \geqslant 1.27$ (MeV),

$$f_1(E_n) = \left((1-x_p^2)^{1/2}\left\{1-\left[1-\left(\frac{b}{\ell_p}\right)^2\right]^{1/2}\left(1+0.392\,\frac{b}{\ell_p}\right)\right\}\right)\left[1-\frac{4}{\pi}\left(\frac{\ell_T}{2b}\right)\right]^{(1-\bar{\mu}_T^2)^{1/2}} ,$$

$$x_p = \frac{1}{(3)^{1/2}}\left(\frac{E_n}{3E_n+3.056}\right)^{1/2} , \quad E_p = 0.586\,E_n + 0.574 \text{ (MeV)}.$$

All other quantities are the same as those in case 1:

$$f_2(E_n) = 1 - \frac{4}{\pi}\left(\frac{\ell_{He}}{2b}\right), \quad 0 \leqslant E_n \leqslant 10,$$

$$\ell_{He} = \frac{1.07}{10}\left(7E_{He} + \frac{6.7}{3}E_{He}^2\right)^* ,$$

E_{He} is from $E_{He} = \frac{3E_n}{8\pi}\left(\frac{8}{3} - I_2\right)$,

$$I_2 = \int_{-1}^{1} \Xi(\mu_{c.m.})\mu_{c.m.}\,d\mu_{c.m.} , \quad \Xi(\mu_{c.m.}) = \int_0^{\frac{\pi}{2}} (1-K^2\sin^2\theta)^{1/2}d\theta$$

$$K = [1 - \tfrac{1}{2}(1-\mu_{c.m.})]^{1/2},$$

---

* The origin of these formulas is discussed later in this section.

$$f_3(E_n) = 1 - f_2(E_n),$$

$$p(E) = \frac{16\pi}{3E_j\sigma_S} \sum_{\ell=0}^{3} a_\ell(E_j) P_\ell \left(1 - \frac{8E}{3E_j}\right) ,$$

$$P(E \rightarrow E_i) = \left[\frac{1}{E_b^2 E_i^2} (E_b E^2 - \frac{2}{3} E^3) + \frac{E^2}{2E_L E_i^2} + \frac{1}{2E_L}\right] ,$$

$$E_b = 1.14 \text{ (MeV)} , \quad E_L = 4.65 \text{ (MeV)},$$

$$\Delta_i E = 0.06 \text{ (MeV)}.$$

The formulas for ℓ_p, E_p, ℓ_T, E_T, b, and L are calculated as follows.

Range formula[7,8]

For the same particles we assume

$$\left(\frac{dE}{d\xi}\right)_{He^3} = \left(\frac{dE}{d\xi}\right)_{He^4}$$

$$\rho_{He^4} R_{He^4} = \rho_{He^3} R_{He^3} ,$$

where R_{He^4} = range in He^4,
R_{He^3} = range in He^3,

therefore

$$R_{He^4} = \frac{\rho_{He^3}}{\rho_{He^4}} R_{He^3} = \frac{1.66\times10^{-4} (g/cm^3)}{1.78\times10^{-4} (g/cm^3)} R_{He^3}$$

and

$$R_{He^4} = \frac{1}{1.07} R_{He^3} .$$

The calculation of E_b and E_L is as follows:

Counter sensitive length L_{10} = 3.5 in. $\times$2.54 = 8.89 cm,

Counter sensitive radius $b_{10} = \frac{15}{32}$ in. $\times$2.54 = 1.16 cm.

The gas in the sensitive volume is at p = 10 atmosphere; then the above values equivalent to values for standard pressure (i.e., p = 1) will be

$$L_1 = L_{10} \times p = 8.89 \times 10 = 88.9 \text{ cm},$$
$$b_1 = b_{10} \times p = 1.16 \times 11.6 \text{ cm}.$$

These values are in He^3 gas; their equivalent values in He^4, according to $R_{He^4} = R_{He^3}/1.07$, will be

$$L = \frac{88.9}{1.07} = 83.1 \text{ cm},$$

$$b = \frac{11.6}{1.07} = 10.84 \text{ cm}.$$

For the proton case, from Figs. 39 and 40, $E_b = 0.85$ MeV, $E_L = 3.05$ MeV.

For the case of the He^3 nucleus we estimate as follows.

According to the formula for different particles in the same gaseous medium,

$$R_{He^3} \text{ in } He^4 (E) = \frac{M_{He^3}}{M_p} R_p \text{ in } He^4 \left(\frac{M_p}{M_{He^3}} E\right),$$

therefore

$$R_{He^3} \text{ in } He^4 (E) = 3 R_p \text{ in } He^4 \left(\frac{1}{3} E\right)$$

and

$$R_{He^3} \text{ in } He^4 (E) = \frac{R_{He^3} \text{ in } He^3}{1.07},$$

therefore

$$L_{He^3} \text{ in } He^4 = \frac{88.9}{1.07} = 83.1 \text{ cm},$$

$$b_{He^3} \text{ in } He^4 = \frac{11.6}{1.07} = 10.84 \text{ cm}.$$

The equivalent proton range of L in He^4 is

$$R_{p,L} \text{ in } He^4 \left(\frac{1}{3} E\right) = \frac{1}{3} \times 83.1 = 27.7 \text{ (cm)}.$$

The equivalent proton range of b in He^4 is

$$R_{p,b} \text{ in } He^4 \left(\frac{1}{3} E\right) = \frac{1}{3} 10.84 = 3.61 \text{ (cm)}.$$

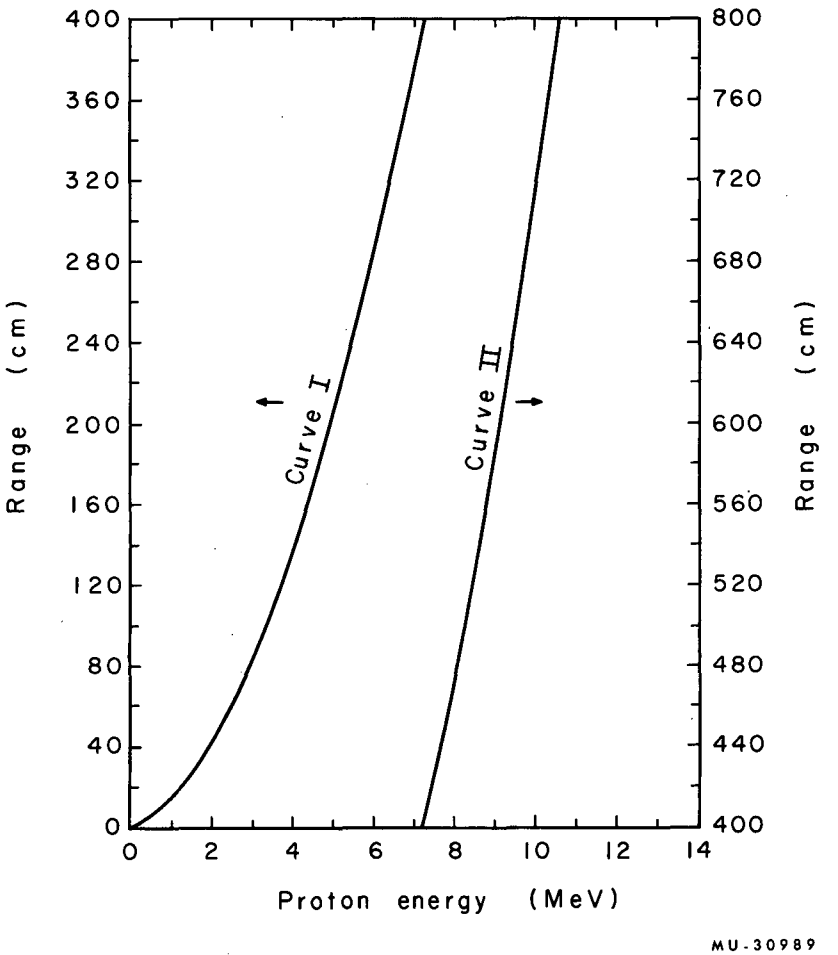

Fig. 39. Range of protons in He at 15°C and 760 mm Hg (range, 0 to 800 cm; curves from references 7 and 8).

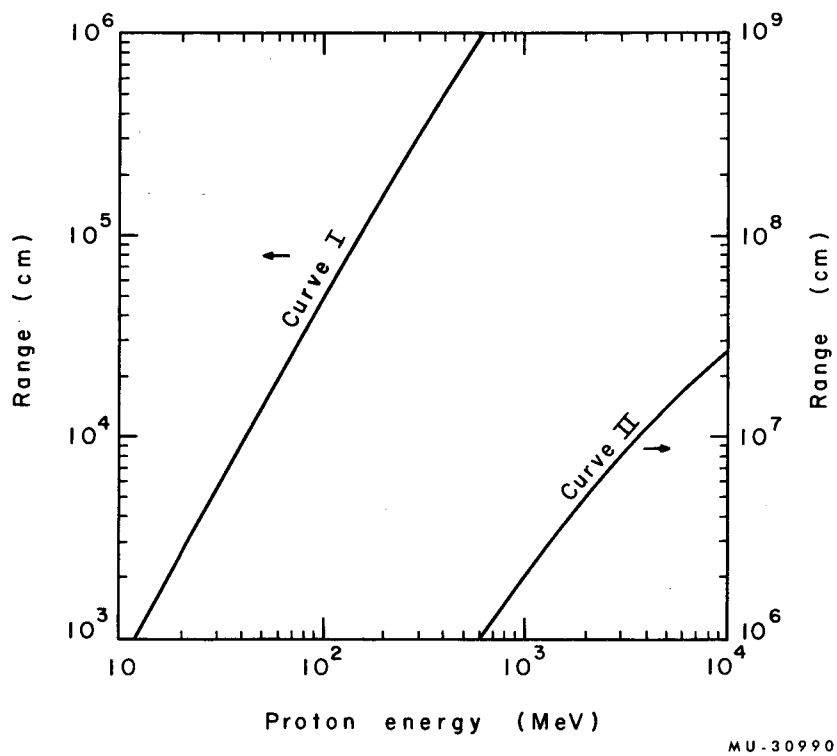

Fig. 40. Range of protons in He at 15°C and 760 mm Hg (range, 10^3 to 10^9cm; curves from references 7 and 8).

From Figs. 39 and 40,

$$\frac{1}{3} E_L = 1.55 \text{ (MeV)}, \qquad \frac{1}{3} E_b = 0.38 \text{ (MeV)},$$

therefore

$$E_L = 4.65 \text{ (MeV)}, \qquad E_b = 1.14 \text{ (MeV)}.$$

For the case of pure He^3 gas, the range of particles can be calculated from the information of range - energy relationship of protons in He^4 by assuming

$$\left(\frac{dE}{d\xi}\right)_{He^3} = \left(\frac{dE}{d\xi}\right)_{He^4} ,$$

therefore

$$R_{He^3} = \frac{\rho_{He^4}}{\rho_{He^3}} R_{He^4} = \frac{1.78\times10^{-4}(g/cm^3)}{1.66\times10^{-4}(g/cm^3)} R_{He^4} ,$$

or

$$R_{He^3} = 1.07 R_{He^4} .$$

For the convenience of machine computation the curves up to 10 MeV on Figs. 39 and 40 may be approximated by

$$R_{He^4} = 7E + 6.7 E^2.$$

D. Comparison of Results

Figure 37 is replotted in Fig. 38 along with those curves for PuF_4 neutron sources from different observers.[9] The curves of PuF_4-3 and PuF_4-2 are obtained by Tochilin[9] by using an emulsion technique, while PuF_4-2 is a Hanford source. The PuF_4-3 is described in Table I, reference 9.

It is seen that the curve obtained here agrees within statistical variations with the curve PuF_4-3 for most energies. However there are some differences observed in the range from 0.4 to 0.8 MeV. The possible reasons for this disagreement are as follows:

(a) A moderated PuBe source was used to determine the response of the He^3 detector to thermal neutrons. This measurement was normalized and used to subtract the thermal-neutron background. There is uncertainty in the distribution of thermal neutrons from the moderated PuBe source and the thermal-neutron spectrum that was acutally present when the PuF_4 source was measured.

(b) Range straggling in emulsion technique increases rapidly in this low-energy range.[10]

It is also seen that this method, in principle, is able to predict neutron distributions down to zero neutron energy if a proper thermal distribution is taken concurrently and subtracted, whereas the emulsion method is unable to do this.

Table II. Ranges of protons in helium and energy losses for 15°C and 760 mm of Hg.[a]

E(MeV)	Helium (I = 44 eV) Energy loss $(\frac{dE}{dx})$ (MeV/cm)	Range (cm)
0	0	0
1	4.75985×10^{-2}	1.3030×10^{1}
2	2.80637	
3	2.00607	8.4160
4	1.61918	
5	1.35183	2.0778×10^{2}
6	1.16537	2.8769
7	1.02733	3.7930
8	9.20701×10^{-3}	4.8229
9	8.35660	5.9645
10	7.66136	7.2155
11	7.08158	
12	6.59015	1.0039×10^{3}
13	6.16793	
14	5.80097	1.3281
15	5.47889	
16	5.19375	1.6931
17	4.93944	
18	4.71110	2.0980
19	4.50487	
20	4.31764	2.5419
25	3.59050	
30	3.08987	5.3241
35	2.72299	
40	2.44195	8.9943
45	2.21941×10^{-3}	
50	2.03861	1.3498×10^{4}
55	1.88867	
60	1.76226	1.8791
65	1.65406	
70	1.56046	2.4736
75	1.47862	
80	1.40644	3.1597
85	1.34229	
90	1.28488	3.9046
95	1.23320	
100	1.18642	4.7154
125	1.00617	
150	8.83659×10^{-4}	9.6737
175	7.94925	
200	7.27717	1.5955×10^{5}
225	6.75029	
250	6.32684	2.3356
275	5.97928	
300	5.68919	3.1712
325	5.44364	
350	5.23335	4.0893
375	5.05144	
400	4.89271	5.0787
425	4.75315	
450	4.62963	6.1303
475	4.51967×10^{-4}	
500	4.42128	7.2363×10^{5}
550	4.25293	
600	4.11470	9.5859
650	3.00067	
700	3.90293	1.2085×10^{6}
750	3.82084	
800	3.75057	1.4701
850	3.69004	
900	3.63760	1.7410
950	3.59196	
1000	3.55206	2.0194
1500	3.33866	
2000	3.27707	4.9940
2500	3.26866	
3000	3.28242	8.0499
3500	3.30613	
4000	3.33429	1.1074×10^{7}
4500	3.36423	
5000	3.39457	1.4046
5500	3.42457	
6000	3.45387	1.6967
6500	3.48228	
7000	3.50971	1.9839
7500	3.53614	
8000	3.56157×10^{-4}	2.2666×10^{7}
8500	3.58604	
9000	3.60960	2.5456
9500	3.63227	
10000	3.65412	2.8209

[a]These data are from references 7 and 8.

ACKNOWLEDGMENTS

This work was conducted under the guidance of Dr. Roger W. Wallace of the Lawrence Radiation Laboratory at Berkeley, and the author would like to thank him for his support, encouragement, and advice throughout.

Of course, as indicated by the many "daggers" in the text, I owe a great debt of gratitude to Dr. W. K. Brown; in a sense my work can be considered at an extension of his work.

The author also wishes to express his gratitude to Mr. Willis R. Young for his constant discussions and suggestions.

This work was done partly under the auspices of the U. S. Atomic Energy Commission, and partly under U. S. Air Force contract AF 29 (601) 2784.

APPENDICES

A. Computer Program

The actual inversion calculation is carried out by a Fortran program. This program utilizes the principles and formulas given in Subsec. VI.C. The calculation takes the following steps.

1. Calibration

When a raw (pulse-height) spectrum is obtained by using the He^3 detector incorporated with a multiple-channel analyzer, the spectrum is first calibrated to a neutron energy scale. Let

V_B = bias voltage of this spectrum (volts),
V_c = voltage per channel (volts/channel),
n = channel number of the spectrum,
N = top channel number of the spectrum,
E = energy of charged particles (e.g., protons and tritons in this detector) per volt, MeV/volt (this data is from the actual calibration by known energy source).

Then the thermal-neutron energy is calibrated at channel number n_0; then

$$(n_0 V_c + V_B) E = Q,$$

where $Q = 0.764$ MeV, the reaction energy of $He^3(n, p)T$, or

$$n_0 = \frac{\frac{Q}{E} - V_B}{V_c}.$$

Thus the energy of thermal neutrons, E_0, corresponds to channel number n_0, and any other neutron energy, E_n, is located by taking

$$E_n = (n - n_0) V_c E \text{ (MeV)}.$$

The top channel of the spectrum, i.e., the channel in which the maximum energy is recorded, is located at N; the value of the energy is E_N(MeV). From this E_N we can start the inversion calculation.

2. Programming the Effect of Deuterons $C_d(j \to i)$

If $E_N \geq 4.36$ MeV, the threshold energy of the $He^3(n, d)D$ reaction $C_d(j \to i)$ should first be computed. The Fortran program uses a formula which expresses the number of counts at the channel corresponding to an energy E_i from deuterons produced by neutrons of energy E_j:

$$C_d(j \to i) = \left\{ \frac{C_j \, \sigma_{n,d}(E_j) \, f_5(E_i)}{\sigma_{n,p}(E_j) \, f_1(E_j)} + \int_{E_j}^{E_N} \frac{C(E) \, \sigma_{n,d}(E) \, f_6(E)}{\sigma_{n,p}(E) \, f_1(E)} \, P(E \to E_i) \, dE \right\},$$

where

C_j is the raw-spectrum data at channel j,

$C(E)$ is the raw-spectrum data at energy E,

$\sigma_{n,d}(E_j)$ is the He^3 n, d reaction cross section (data from Fig. 24 at E_j),

$\sigma_{n,p}(E_j)$ and $\sigma_{n,p}(E)$ are the He^3 n, p reaction cross section (data from Fig. 25 at $E = E_j$ and $E = E$, respectively),

$f_1(E)$ and $f_1(E_j)$ are from Eqs. (VI. 2), (VI. 5) to (VI. 10) evaluated at $E = E_j$ and $E = E$, respectively,

$f_5(E_i)$ is from Eqs. (VI. 16) to (VI. 19) at $E = E_i$,

$f_6(E)$ is from Eq. (VI. 20),

$P(E \to E_i)$ is from Eq. (VI. 22),

For programming, the calculation takes the following steps:

(1) Let $E_j = E_N$, where E_N is the top channel of the raw spectrum and the raw spectrum is denoted by C.

(2) Use the formula $C_d(j \to i)$ to compute $C_d(N \to i)$ for $i = N-1$.

(3) Calculate C (at $E = E_{N-1}$) $- C_d(N \to N-1) = \overline{C}_d(E_i = E_{N-1})$, where the energy (or the channel number) inside the brackets indicates the energy (or the number of the channel) where these C's are evaluated, and $\overline{C}_d$ is the new spectrum which will be used in later computations.

(4) Repeat steps (1), (2), and (3) but change i to $i-1$.

(5) Repeat steps (1), (2), (3), and (4), decreasing i by 1 each time until $E_i = 0$.

(6) Replace original C by $\overline{C}$ just calculated.

(7) Repeat the steps from (1) to (6) by changing j to $j-1$, with $\overline{C}$ as "new" raw spectrum.

(8) Repeat step (7), decreasing j by 1 each time until $E_j = 4.36$ MeV, the threshold energy of the n, d reaction.

The desired data are tabulated in the following form.

Table A.I

$\overline{C}_d(i)$ \ E_i / E_j	E_{N-1}	E_{N-2}	. . .	E = 4.36	. . .	E = 0
E_N						
E_{N-1}						
⋮						
E = 4.36						

Data in the dashed-line spaces will be the resultant spectrum after unfolding the deuterium effect. If $E_N < 4.36$ MeV, the above calculation should be omitted.

3. Program for $C_{He}(j \to i)$

If $E_N \geq 4.36$ MeV, the $C_d(j \to i)$ should be calculated first; otherwise, this calculation can be omitted. The Fortran program for the calculation of $C_{He}(j \to i)$ uses the formula

$$C_{He}(j \to i) = \left[\frac{C_j \, \sigma_S(E_j)}{\sigma_{n,p}(E_j) f_1(E_j)} \left\{ f_2(E_j) p(E_i) + f_3(E_j) \int_{E_i}^{\frac{3}{4}E_j} p(E) P(E \to E_i) \, dE \right\} \right] \Delta_i E,$$

where

C_j is the raw spectrum at E_j,
$f_2(E_j)$ is from Eqs. (VI. 11) to (VI. 14),
$f_3(E_j)$ is from Eq. (VI. 15),
$p(E_i)$ or $p(E)$ is from Eq. (VI. 21) [also refer to Eq. (IV. 1) and Fig. 20],
$P(E \to E_i)$ is from Eq. (VI. 22).

All other quantities follow from Appendix Subsec. A. 2 except $f_1(E_j)$ which is from the following two cases:

Case 1. $E_N \leq E_{crit}$ then $f_1(E_j)$ is from Eqs. (VI. 2) and (VI. 3).
Case 2. $E_N > E_{crit}$ then $f_1(E_j)$ is from Eqs. (VI. 2) and (VI. 5).

Case (2) should be used first as the unfolding process goes down from top channel if $E_N > E$ is critical. This E_{crit} is defined as the energy E_n where

$$\left(1 - \frac{2}{x_p}\left\{\frac{\ell_{p_1}}{2b}\left[1 - \left(\frac{\ell_{p_1}}{2b}\right)^2\right]^{1/2} + \sin^{-1}\left(\frac{\ell_{p_1}}{2b}\right)\right\}\right) = \left(\left(1 - x_p^{\,2}\right)^{1/2}\left\{1 - \left[1 - \left(\frac{b}{\ell_{p_2}}\right)^2\right]^{1/2}\right\}\left(1 + 0.392\,\frac{b}{\ell_{p_2}}\right)\right),$$

where ℓ_{p_1} is evaluated from the energy given by Eq. (VI. 4),

$$E_p = 0.505\ E_n + 0.450\ (\text{MeV}),$$

and ℓ_{p_2} is evaluated with energy E_p given by Eq. (VI. 7),

$$E_p = 0.586\ E_n + 0.574\ (\text{MeV})$$

$$x_p = \frac{1}{(3)^{1/2}} \left(\frac{E_n}{3E_n + 4Q_{n,p}} \right)^{1/2}, \quad Q_{n,p} = 0.764\ \text{MeV}, \text{ Eq. (VI. 6)}.$$

It is seen that E_{crit} should be evaluated numerically with a known filling-gas pressure, since ℓ_p is a function of both pressure and energy. Below E_{crit} case (1) is then used.

For programming, the calculation takes the following steps:

(1). Let $E_j = E_N$, the top channel of the raw spectrum (defined as C)

$$E_i = \frac{3}{4}\ E_N.$$

(2). Use the $C_{He}(j \rightarrow i)$ formula to compute the contribution of spectrum at $E = E_i = \frac{3}{4} E_N$ due to the particles of $E_j = E_N$.

(3). Calculate C (at $E_i = \frac{3}{4} E_N$) - $C_{He}(j \rightarrow i)$ just calculated from (2). Let $\bar{C}\ (E_i = \frac{3}{4}\ E_N) = C - C_{He}$. This $\bar{C}$ is the new spectrum at $E = E_i = \frac{3}{4} E_N$, which will be used in later computations.

(4). Repeat steps (1), (2), and (3) but change i to i-1; i.e., E_{i-1} replaces E_i.

(5). Repeat steps (1), (2), (3), and (4), lowering i by 1 each time, until $E_i = 0$.

(6). Repeat steps (1) to (5) by changing j to j-1; i.e., $E_{j-1} = E_{N-1}$ replaces $E_j = E_N$. Also use $\bar{C}$ to replace C as the new input spectrum.

(7). Repeat step (6), lowering j and 1 each time until $E_j = 0$.

Now the computation for this process is completed. The required data are listed in the following table, noting that the $\overline{C}_{He}$ is the result of step (7) for each E_j. The data in spaces marked with a dashed line are the data of the unfolded spectrum.

Table A. II.

$\overline{C}_{He}$ \ E_j / E_i	E_N	E_{N-1}	. . .	0
$\frac{3}{4} E_N$				
$\frac{3}{4} E_{N-1}$				
. . .				
0				

4. Program for $C_p(i)$

The Fortran program for the computation of $C_p(i)$ uses the formula

$$C_p(i) = \int_{E_i}^{E_N} \frac{C[1 - f_1(E)]}{f_1(E)} P(E \rightarrow E_i)\, dE ,$$

where C is the raw-spectrum data. All other quantities are defined in Appendix A.2 and A.3.

For programming, the calculation takes the following steps:

(1). Let E_N = energy of top channel of the raw spectrum which is denoted by C.

(2). Use the above formula to calculate $C_p(i)$ at $E_i = E_{N-1}$.

(3). Compute $C(E_{N-1}) - C_p(E_i = E_{N1})$ just calculated $= \bar{C}(E_{N-1})$. This $\bar{C}_p$ is the new input spectrum for later calculation.

(4). Repeat the steps (1), (2), and (3) but change i to i-1.

(5). Repeat the steps (1), (2), (3), and (4), lowering i by 1 each time until $E_i = 0$.

(6). Repeat the steps from (1) to (5) by changing E_N to E_{N-1} using $\bar{C}(E_n)$ as the input spectrum.

(7). Repeat step (6) lowering N by 1 each time until $E_N = 0$.

Now the computation for this process is completed. The required data are listed in the following table, noting that $\bar{C}_p$ is the result of step (7). The data in spaces marked with a dashed line are the data of the unfolded spectrum.

Table A. III.

$\bar{C}_p$ \ E_N	E_N	E_{N-1}	. . .	0
E_{N-1}				
E_{N-2}				
. . .				
0				

5. Resultant Spectrum

The resultant spectrum can be programmed by using the following formula:

$$
\begin{aligned}
C_0 &= C - \left[(C - \overline{C}_d) + (C - \overline{C}_{He}) + (C - \overline{C}_p)\right] \\
&= C - \left\{[C-[C-C_d(j\rightarrow i)]\right\} + \left\{C-[C - C_{He}(j\rightarrow i)]\right\} + \left\{C-[C - C_p(i)]\right\} \\
&= C - [C_d(j\rightarrow i) + C_{He}(j\rightarrow i) + C_p(i)] \\
&= \overline{C}_d + \overline{C}_{He} + \overline{C}_p - 2C,
\end{aligned}
$$

where

C_0 is the desired spectrum at the corresponding channel,
$\overline{C}_d$, $\overline{C}_{He}$, and $\overline{C}_p$ are the spectra from respectively,
C is the raw spectrum.

B. Sample Calculation

Based on the methods mentioned in Appendix A, the actual computation procedures are presented here for the example mentioned in Sec. VII.

1. Neutron Energy-Scale Calibration

The raw spectrum plotted in Fig. 32 is first calibrated with the neutron energy scale E_n. The method of calibration follows from Appendix A.1.

The bias voltage for that spectrum is 2 V, the calibrated energy is 30 keV per channel, and the analyzer channel voltage is 1 volt per channel. Therefore the channel n, corresponding to thermal-neutron energy, is from $(n\times 1 + 2)\ 0.03 = 0.764$, or $n = 24$. That is, channel 24 is equivalent to thermal-neutron energy, and the top channel (100) is then identified as 2.28 MeV.

2. Calculation of ℓ_p, ℓ_T, ℓ_{He}, E_b, and E_L

The actual computations of these quantities are carried out in Subsec. VII. C.

3. Determination of E_{crit}

Before computing the C's mentioned in Appendix A, the value of E_{crit} must be evaluated numerically. Here for a filling-gas pressure in the detector of 10 atm, E_{crit} is machine-computed to be 1.27 MeV.

4. $\overline{C}_{He}$ Data

Since $E_N = 2.28$ is less than 4.36 MeV, the effect of $He^3(n,d)D$ is omitted. By using the method mentioned in Appendix A.3, a set of data can be obtained and arranged in the form of Table II in the same appendix. Those data in dashed-line spaces are plotted as Fig. 33.

5. $\overline{C}_p$ Data

By using the method mentioned in Appendix A.4, a set of data can be obtained and arranged in the form of Table III in the same appendix. Those data in dashed-line spaces are plotted as Fig. 34.

6. Resultant Spectrum

By using the method mentioned in Appendix A.5, the resultant spectrum is obtained as plotted in Fig. 36.

7. Corrected Neutron Spectrum

The corrected neutron spectrum is obtained by dividing the above resultant spectrum by η, the overall spectrometer efficiency. The η is given by Eqs. (VI.1) et sed. The corrected neutron spectrum for this example is plotted in Fig. 37.

8. Comparison of Spectra

Figure 35 shows a comparison of spectra obtained from the preceding Subsecs. 4, 5, and 6, together with the original raw spectrum. From this comparison, the effect due to any particular process can be seen clearly. However this is not a necessary step for inversion calculation.

9. Comparison of Results

This is not a necessary step for the inversion calculation either. The TNC curve in Fig. 38 is a replot of Fig. 37 by normalizing the peak value of the curve in Fig. 37 to the same peak value of the curve PuF_4-3 in Fig. 38.

REFERENCES

1. R. Batchelor, R. Aeves, and T. H. R. Skyreme, Helium-3 Filled Proportional Counter for Neutron Spectrometer, Rev. Sci. Instr. 26, 1037 (1955).
2. John N. Green, Preliminary Testing of a Proportional Counter for Neutron Spectroscopy with Helium-3, University of California Radiation Laboratory Report UCRL-8274, April 1958 (unpublished).
3. Alden R. Sayres, Interaction of Neutrons with He^3 (Ph. D. Thesis), Columbia University Report CU-PNPL-200, March 7, 1960 (unpublished).
4. S. B. Bloom, E. Riley, and B. J. Toppel, A High Pressure Proportional Counter for Fast Neutron Spectroscopy, Brookhaven National Laboratory Report BNL-358, June 1955 (unpublished).
5. Wilbur Knight Brown, A Helium-3 Neutron Spectrometer With Extended Energy Range: Part II, Method of Energy-Range Extension, Lawrence Radiation Laboratory Report UCRL-6911, May 1962 (unpublished).
6. William R. Mills, Jr., Richard L. Caldwell, and Ira L. Morgan, Low Voltage He^3-Filled Proportional Counter for Efficient Detection of Thermal and Epithermal Neutrons, Rev. Sci. Instr. 33, 886 (1962).
7. Marvin Rich and Richard Madey, Range Energy Tables, University of California Radiation Laboratory Report UCRL-2301, March 1954 (unpublished).
8. W. A. Aron, B. G. Huffman, and F. C. Williams, Range Energy Curves, Lawrence Radiation Laboratory Report UCRL-121 Second Rev., 1949 (unpublished).
9. Eugene Tochilin, Flux and Spectral Measurement of Primary and Moderated Neutron Sources, U. S. Navy Radiological Defense Laboratory Report USNRDL-TR-587, October 1962 (unpublished).
10. Chul Mo Kim, A Theoretical Comparison of 4π Fast-Neutron Spectrometers, Lawrence Radiation Laboratory Report UCRL-9504, November 1960 (unpublished).

This report was prepared as an account of Government sponsored work. Neither the United States, nor the Commission, nor any person acting on behalf of the Commission:

A. Makes any warranty or representation, expressed or implied, with respect to the accuracy, completeness, or usefulness of the information contained in this report, or that the use of any information, apparatus, method, or process disclosed in this report may not infringe privately owned rights; or

B. Assumes any liabilities with respect to the use of, or for damages resulting from the use of any information, apparatus, method, or process disclosed in this report.

As used in the above, "person acting on behalf of the Commission" includes any employee or contractor of the Commission, or employee of such contractor, to the extent that such employee or contractor of the Commission, or employee of such contractor prepares, disseminates, or provides access to, any information pursuant to his employment or contract with the Commission, or his employment with such contractor.